Microbial community biomass, production and grazing along 110°E in the eastern Indian Ocean

Michael Landry, Raleigh Hood, Claire Davies, Karen Selph, David Antoine, Mika Carl, Lynnath Beckley

Deep–Sea Research II 202 (2022) 105134

Contents lists available at ScienceDirect

Deep-Sea Research Part II

journal homepage: www.elsevier.com/locate/dsr2

Microbial community biomass, production and grazing along 110°E in the eastern Indian Ocean

Michael R. Landry [a,*], Raleigh R. Hood [b], Claire H. Davies [c], Karen E. Selph [d], David Antoine [e,f], Mika C. Carl [a], Lynnath E. Beckley [g]

[a] Scripps Institution of Oceanography, University of California at San Diego, La Jolla, CA, 92093-0227, USA
[b] Horn Point Laboratory, University of Maryland Center for Environmental Science, Cambridge, MD, USA
[c] CSIRO Oceans and Atmosphere, Castray Esplanade, Hobart, Tasmania, 7000, Australia
[d] Department of Oceanography, University of Hawai'i at Manoa, Honolulu, HI, 96822, USA
[e] Remote Sensing and Satellite Research Group, School of Earth and Planetary Sciences, Curtin University, Perth, WA, 6845, Australia
[f] Sorbonne Université, CNRS, Laboratoire d'Océanographie de Villefranche, LOV, F-06230, Villefranche-sur-Mer, France
[g] Environmental and Conservation Sciences, Murdoch University, Murdoch, 6150, Western Australia, Australia

ARTICLE INFO

Keywords:
Phytoplankton growth
Production
Microzooplankton grazing
Picoplankton
Prochlorococcus
Heterotrophic bacteria
Subtropical
Tropical

ABSTRACT

We investigated plankton biomass structure, production and grazing rates from temperate to tropical waters (39.5–11.5°S) along the historic 110°E transect in the eastern Indian Ocean (IO) during May–June 2019. The timing captures the seasonal transition from moderate productivity in the subtropical sector to seasonally high primary production in tropical waters as described in IIOE (International Indian Ocean Expedition) studies of the 1960s. Carbon-based estimates of phytoplankton production and microzooplankton grazing were determined from depth profiles of dilution incubations analyzed by flow cytometry and pigments; mesozooplankton biomass and grazing were determined from net sampling and gut fluorescence for the integrated euphotic zone. Phytoplankton biomass varied from 860 to 1740 mg C m^{-2}, averaging 1187 mg C m^{-2} with no latitudinal trend. Mixed-layer C:Chl*a* ranged from 20 to 40 in the nitrogen-rich subtropical front to 100–180 in tropical waters. *Prochlorococcus* increased from 141 to 915 mg C m^{-2} between 39.5°S and 20°S and averaged 700 mg C m^{-2} at lower latitudes. *Synechococcus* and photosynthetic eukaryotes contributed least to biomass (3.6 and 30.5%, respectively) at mid-transect locations (15.5–27.5°S). Dinoflagellates and diatoms were typically rare (28 and 6 mg C m^{-2}, respectively). Among heterotrophs, bacteria averaged 476 mg C m^{-2}, with a subtropical front maximum but no latitudinal trend; ciliates averaged 112 mg C m^{-2}, and mesozooplankton increased significantly south-to-north (131–488 mg C m^{-2}). Phytoplankton production and grazing averaged 466 and 461 mg C m^{-2} d^{-1}, respectively, based on the sums for flow-cytometry measured populations, and 618 and 604 mg C m^{-2} d^{-1}, respectively, based on Chl*a*-determined rates. Our results highlight key relationships that link stocks and process rates across oceanographic provinces of the eastern IO. Production and grazing increased 6–8 fold from south to north. *Prochlorococcus* dominated productivity, and microzooplankton accounted for 85–89% of grazing. Production and grazing were strongly coupled and balanced on average. Over the transect, increasing growth conditions (light and temperature) mainly manifested as more rapid biomass turnover and mesozooplankton biomass accumulation.

1. Introduction

Low-latitude waters of the Indian Ocean (IO) absorb most of the excess heat from the Pacific Ocean that flows through the Indonesian Throughflow (ITF) and have been warming faster than comparable areas of the Atlantic and Pacific (Lee et al., 2015; Desbruyères et al., 2017), with satellite observations also suggesting the largest decline of phytoplankton biomass (Gregg and Rousseaux, 2019). Yet the IO remains the most sparsely studied ocean, with precious little data for evaluating long-term changes in ecosystem structure and function. The last major system-level investigation of the southeastern IO was the International Indian Ocean Expedition (IIOE) of the 1960's. From bimonthly cruises

* Corresponding author.
E-mail address: mlandry@ucsd.edu (M.R. Landry).

https://doi.org/10.1016/j.dsr2.2022.105134
Received 18 October 2021; Received in revised form 19 April 2022; Accepted 12 June 2022
Available online 15 June 2022

conducted along longitude 110°E from August 1962 to August 1963, Australian oceanographers of that era did a remarkable job describing the complexities of regional circulation and forcing (Rochford, 1969, 1977), the distributions of nutrients, phytoplankton chlorophyll and particulate carbon (Humphrey and Kerr, 1969; Newell, 1969; Rochford, 1963), and the seasonal cycles of primary production and mesozooplankton (Jitts 1969; Tranter and Kerr, 1969, 1977), with an emphasis on diverse zooplankton groups and species (McWilliam, 1977; Sakthivel, 1977; Tranter, 1977a,b). Nonetheless, this early effort preceded many key discoveries that constitute the modern foundation of pelagic food web understanding: the revolutionary paradigm of the microbial loop (Azam et al., 1983), ubiquitous and abundant photosynthetic bacteria (Waterbury et al., 1979; Chisholm et al., 1988), dominant grazing roles of protistan microzooplankton (Calbet and Landry, 2004), and even the methodology to make systematic measurements of zooplankton grazing of any kind. While some of these missing food-web components have been considered in the few regional studies since IIOE, those have tended to focus on comparative investigations of distinct mesoscale features and their implications for fisheries recruitment (Waite et al., 2007b, 2019; Wang et al., 2014; Säwström et al., 2014) as well as latitudinal and mesoscale variability along the Leeuwin Current (e.g., Thompson et al., 2011; Lourey et al., 2013; Sutton and Beckley, 2016). Thus, it remains difficult to assess possible decadal changes due to anthropogenic climate impacts or to place the contemporary dynamics of the eastern IO in the context of other well-studied ecosystems.

R/V *Investigator* cruise IN2019_V03 was undertaken as part of IIOE-2 (Second International Indian Ocean Expedition) to improve understanding of physical, biogeochemical and trophic processes across temperate to tropical oceanic waters of the historic 110°E transect, with the goal of providing a modern perspective to facilitate development of regional physical-biogeochemical models (Beckley et al. this volume). As part of this expedition, we conducted sampling and experiments to compare biomass, production and grazing from bacteria to mesozooplankton at 20 stations from 39.5 to 11.5°S. Our study, comprising the first integrated investigation of plankton community structure and food-web dynamics in the eastern IO, was motivated by several basic questions: What are the key relationships that link stocks and process rates across different oceanographic provinces over this broad latitudinal extent? How do they relate to previous IIOE descriptions along 110°E, and, where comparisons can be made, are there indications of significant change over the intervening six decades? How do the measurements and relationships relate to findings from similarly conducted investigations in other tropical and subtropical ecosystems?

2. Materials and methods

2.1. Sampling and experimental set-up

Sampling and experiments were conducted at 20 stations on the 110°E transect from 17 May to June 5, 2019 on *R/V Investigator* cruise IN2019_V03 (Fig. 1a, Table 1). The stations, spaced mostly 1.5° apart from 39.5 to 11.5°S, were occupied on successive days according to a consistent daily schedule, followed by late-night transit between stations. Mean light extinction coefficients for the euphotic zone were determined from PAR (Photosynthetically Active Radiation) profiles in morning (~10:00) CTD hydrocasts. Mesozooplankton net tows were taken at mid-day (~13:30) and 1–2 h after local sunset (~19:30) with a 1-m diameter ring net (0.2-mm Nitex mesh, General Oceanics flowmeter and Senus Ultra time-depth-temperature recorder) towed obliquely through the euphotic zone at a ship speed of 1.5 kt (Landry et al., 2020a). Seawater for microplankton community analyses and to set-up dilution experiments was collected on evening CTD hydrocasts (~21:00) at light depths determined from the morning cast of 76, 32, 18, 7.6, 2.6 and 1.3% of incident PAR, hereafter $\%I_o$, corresponding to the transmission characteristics of six incubator containers described below. Seawater samples (2.3 L) for pigment analyses by high pressure liquid chromatography (HPLC) were also collected on the same evening CTD hydrocasts as samples for microplankton community analyses, but in different bottles and generally at different depths, following a semi-fixed depth plan (e.g., 5, 10, 25, 50, 75, 100 m, etc.). To compare HPLC results from fixed depths to samples collected at light depths, we interpolated measurements from the fixed depths to values at the sampled light depths.

For each light-depth sampled, we prepared a two-treatment dilution experiment (Landry et al., 2008, 2011), with one polycarbonate bottle (2.7 L) containing unfiltered seawater (100%) and the second (diluted) bottle consisting of ~33% whole seawater with filtered water from the same depth. Seawater was filtered directly from the Niskin bottles using a peristaltic pump, silicone tubing and an in-line 0.2-μm Suporcap filter

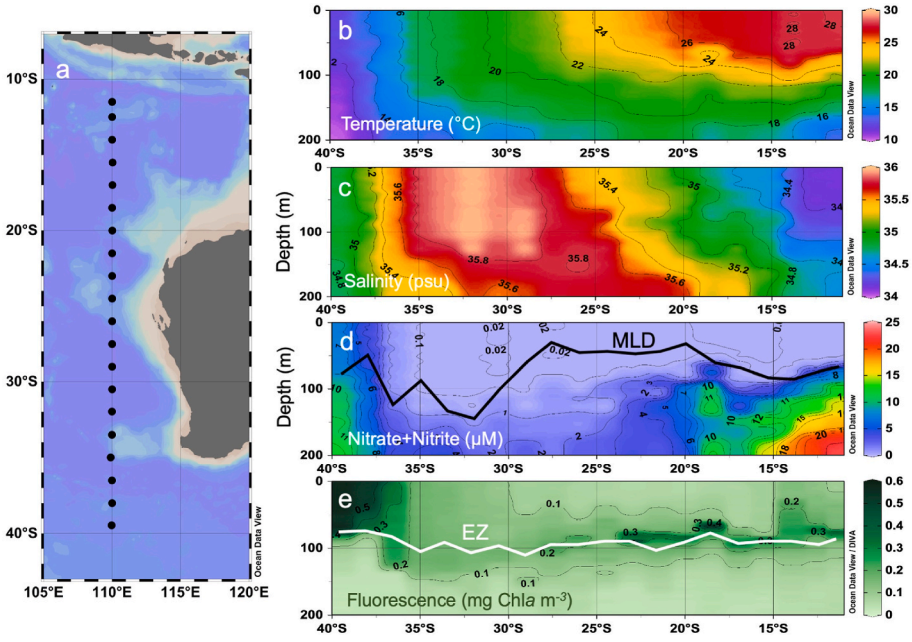

Fig. 1. Station locations and environmental parameter sections from CTD profiles conducted along 110°E. Indonesia is north of 10°S and Australia is to the east in station map (a). Temperature (b), salinity (c) and Chl*a* fluorescence (e) are from continuous CTD instrument measurements averaged at 1-m depth intervals. Nitrate + Nitrite concentrations (d) are from shipboard analyses at discrete sampling depths. Black line in Panel d is Mixed Layer Depth (MLD), defined as the depth at which temperature decreases 0.1 °C below surface values (Landry et al., 2020). White line in Panel e is the Euphotic Zone (EZ), the depth of penetration of 1% of surface irradiance calculated from the mean coefficient of light extinction (PAR) (Landry et al., 2020).

Table 1
Sample collection and incubation conditions for shipboard dilution experiments conducted along the 110°E transect in May–June 2019. Date is the day of sample collection and beginning of the 24-h incubation. Sampling conditions are wind speed (km h^{-1}) and incident PAR (E m^{-2} d^{-1}) during the daytime period of the day of sample collection. Incubation conditions are PAR and mean seawater temperature in the running seawater line over the day of experimental incubation. Parameters were each measured by two instruments. Uncertainties are standard errors of mean values.

Lat (°S)	Date	Sampling Conditions		Incubation Conditions	
		Wind (km h^{-1})	PAR (E m^{-2} d^{-1})	PAR	Temp (°C)
39.5	17 May	16.5 ± 0.2	13.2 ± 0.2	9.8 ± 0.2	13.99 ± 0.09
38.0	18 May	30.9 ± 0.2	9.8 ± 0.2	5.3 ± 0.1	15.33 ± 0.08
36.5	19 May	45.0 ± 0.4	5.3 ± 0.1	20.4 ± 0.1	18.06 ± 0.08
35.0	20 May	40.7 ± 0.1	20.4 ± 0.1	15.2 ± 0.1	18.12 ± 0.05
33.5	21 May	25.8 ± 0.1	15.2 ± 0.1	18.7 ± 0.1	19.16 ± 0.05
32.0	22 May	12.6 ± 0.1	18.7 ± 0.1	16.8 ± 0.4	20.26 ± 0.05
30.5	23 May	18.2 ± 0.2	16.8 ± 0.4	19.0 ± 0.5	20.69 ± 0.05
29.0	24 May	27.7 ± 0.2	19.0 ± 0.5	17.7 ± 0.4	21.85 ± 0.05
27.5	25 May	36.2 ± 0.1	17.7 ± 0.4	28.4 ± 1.9	23.31 ± 0.05
26.0	26 May	36.2 ± 0.3	28.4 ± 1.9	25.8 ± 1.1	24.06 ± 0.05
24.5	27 May	17.8 ± 0.0	25.8 ± 1.1	27.6 ± 0.9	24.88 ± 0.05
23.0	28 May	12.7 ± 0.3	27.6 ± 0.9	34.4 ± 1.8	25.58 ± 0.05
21.5	29 May	19.4 ± 0.3	34.4 ± 1.8	34.3 ± 2.4	26.44 ± 0.05
20.0	30 May	19.2 ± 0.4	34.3 ± 2.4	37.4 ± 0.8	26.88 ± 0.05
18.5	31 May	29.2 ± 0.1	37.4 ± 0.8	37.3 ± 0.8	27.10 ± 0.05
17.0	1 June	40.7 ± 0.1	37.3 ± 0.8	35.7 ± 1.6	27.31 ± 0.04
15.5	2 June	36.5 ± 0.0	35.7 ± 1.6	35.8 ± 1.0	28.01 ± 0.01
14.0	3 June	31.2 ± 0.1	35.8 ± 1.0	36.0 ± 0.9	28.07 ± 0.05
12.5	4 June	24.9 ± 0.1	36.0 ± 0.9	37.6 ± 3.4	28.11 ± 0.05
11.5	5 June	19.4 ± 0.4	37.6 ± 3.4	21.1 ± 0.5	28.06 ± 0.05

capsule that had previously been acid washed. Dilution bottles were first given a measured volume of filtered water and then gently filled to the top with unscreened water from the Niskin bottles to avoid physical damage to fragile protists (Gifford, 1988; Lessard and Murrell, 1998), and no nutrients were added. Lessard and Murrell (1998) demonstrated that added nutrients were not needed for rate linearity in oligotrophic systems, while added nutrients often resulting in erratic results and depressed grazing. After preparation, each bottle was subsampled for flow cytometric (FCM, 2 mL) analyses of initial concentrations and volumetric dilution factors. The paired bottles from each depth were placed in their respective incubator boxes for 24 h, cooled with constant high flow from the ship's running seawater line. The incubators were covered to protect from deck lighting during nighttime operations and received full solar lighting during the daytime.

Each incubator was constructed with an outer box and lid of clear, light blue (#2069) or dark blue (#2424) Plexiglas and inner panels and lids of neutral density acrylic. Samples of each component were analyzed separately with a Cary 300 spectrophotometer for spectral transmission from 375 to 750 nm, and the outer box colors and inner filters were matched to mimic the reduced transmission and blue spectral shift with depth. After construction, each incubator was calibrated for exact % transmission with a 4π PAR sensor inside the water-filled incubators relative to simultaneous measurements of incident PAR with a 2π sensor.

2.2. Environmental measurements

Temperature and salinity were measured during sample collection by CTD sensors and direct shipboard analyses (Guildline 8400B salinometer). Incubation temperature is the mean of two sensors in the ship's running seawater line, recorded at 5-min intervals and daily averaged. Daily incident solar light (PAR, moles photon flux m^{-2} d^{-1} = E m^{-2} d^{-1}) is the mean of two Licor LI-190 PAR sensors positioned on the ship's port and starboard sides, integrated over the photoperiod from measured μE m^{-2} s^{-1} at 5-min intervals. Wind speed was also measured by two instruments (RM Young 05106 Propellor anemometer, Gill WindObserver II Ultrasonic anemometer) and averaged for the daytime as an indicator of day-to-day variability in wind mixing energy. Nutrients were analyzed on board by the CSIRO hydrochemistry group using a Seal AA3HR segmented-flow autoanalyzer (Rees et al., 2018). Analyses were standardized to certified reference material and had detection limits of 0.02 μM for nitrate + nitrite and phosphate, 0.2 μM for silicate, and 0.01 μM for ammonium.

2.3. Flow cytometric analyses

Picophytoplankton FCM samples were preserved with 3% paraformaldehyde and frozen at −80 °C. Thawed samples were stained with Hoechst 34,580 (1 μg mL^{-1}; Monger and Landry, 1993) and analyzed at a flow rate of 30 μL min^{-1} with a Beckman-Coulter CytoFLEX-S cytometer with 4 lasers (Selph, 2021). Side scatter, forward angle light scatter (FALS) and fluorescence signals were measured using laser excitation (EX)/emission (EM) filters of EX375/EM450 ± 45 for Hoechst-stained DNA, EX488/EM690 ± 50 for chlorophyll, and EX561/EM585 ± 42 for phycoerythrin. Listmode files (FCS 3.0) were analyzed with FlowJo software (v.10.6.1) for abundances of *Prochlorococcus* (PRO), *Synechococcus* (SYN), photosynthetic eukaryotes (EUK) and heterotrophic bacteria (HBAC), as well as their population-average fluorescence and scatter signals normalized to fluorescent microbead standards.

Population carbon estimates were determined from cell abundances and mean cell carbon scaled to relative cell sizes. For PRO, we assumed a base value of 32 fg C $cell^{-1}$ (Garrison et al., 2000) and a mean diameter of 0.65 μm for subtropical surface waters. Base values for SYN and EUK were scaled proportionally to 155 and 3150 fg C $cell^{-1}$ for cells of 1.1 and 3.0 μm diameters, respectively. For HBAC, we used a base value of 11 fg C $cell^{-1}$ (Garrison et al., 2000). To account for cell carbon variability due to cell size differences along the transect and with depth, we used the bead-normalized FALS ratio $(FALS_i/FALS_b)^{0.55}$ as a measure of the relative cell biovolume in sample *i* compared to the base value *b* (Landry et al., 2003), which comes from the near-linear relationship between FALS and Mie scattering cross section for cells in the submicron-micron size range (DuRand and Olson, 1996). For chlorophyll-containing populations, mean bead-normalized red fluorescence captured by filter EM690 ± 50 was used as a relative measure of cell Chl*a* content.

2.4. Pigment and microscopical analyses

Initial and final samples (500 mL) for shipboard fluorometric Chl*a* analyses of dilution experiments were filtered onto GF/F filters and extracted with 90% acetone in a −20 °C freezer for 24 h. Extracted samples were warmed to room temperature in the dark and analyzed on a Turner Designs model 10 fluorometer calibrated against a pure Chl*a* standard (Strickland and Parsons, 1972).

Samples (2.3 L) for analyses of chlorophyll and carotenoid pigments by high-pressure liquid chromatography (HPLC) were concentrated onto Whatman GF/F filters under low vacuum pressure, immediately frozen in liquid nitrogen, and stored at −80 °C. The samples were extracted for 2 h in 100% methanol, disrupted by sonication, clarified by GF/F filtration and analyzed by HPLC (Agilent Technologies 1200 Series) at the analytical facility of the Institut de la Mer de Villefranche (CNRS-France) according to procedures described in Ras et al. (2008).

Seawater samples (250 mL) were also preserved with 5% acid Lugol's solution for microscopical analyses of select protists by the Utermöhl method (Lund et al., 1958). For the present analysis, samples from the upper three sampling depths (76, 33 and 18% I_o) were volumetrically combined to produce one sample representing the upper euphotic zone. Over a process taking several days, the combined sample was measured for total volume in a volumetric cylinder, settled for 24 h, concentrated by suctioning off the upper water and ultimately settled and analyzed in an Utermöhl chamber. All recognizable ciliates, dinoflagellates and diatoms on the resulting slide were imaged on a Zeiss AxioVert 200 M inverted microscope at 200X magnification using brightfield illumination and processed using Image Pro software. For ciliates, we calculated carbon biomass as pg C = 0.19 × BV (Putt and Stoecker, 1989) based on cell biovolumes (BV, μm^3) from length and width measurements and the most appropriate cell shapes. For dinoflagellates and diatoms, C biomass was computed from the equations of Menden-Deuer and Lessard (2000). Measured biomass concentrations for the upper EZ were extrapolated to the depth of the full EZ assuming uniform mixing.

2.5. Microbial growth and grazing rates

We determined rate profiles for phytoplankton growth (μ, d^{-1}) and microzooplankton grazing (m, d^{-1}) from each pair of dilution experiment bottles and for each FCM population and Chl*a* according to the following equations:

$$m = (k_d - k)/(1 - D) \text{ and } \mu = k + m$$

where k_d and k are the measured net rates of change between initial and final concentrations in the diluted and undiluted treatments, respectively, and D (= 0.33) is the portion of unfiltered water in the dilution treatment (Landry et al., 2008; Selph et al., 2011). Rate estimates assume comparable growth rates in dilution treatments and proportional grazing relative to dilution, consistent with the expected close coupling of production, grazing and nutrient remineralization in microbial communities of oligotrophic systems. Rate estimates for FCM populations are from cell abundances. Chl*a*-based rates are from fluorometer readings and mean acid ratios from initial and final treatments at each experimental depth, with growth rates corrected for change in cell Chl*a*: C content, determined as Ln $[(RF:C)_{final}/(RF:C)_{init}]$, where RF and C are community totals for bead-normalized red fluorescence and carbon, respectively. Carbon-based estimates of phytoplankton production (PROD) and microzooplankton grazing (MICRO GRAZ) were calculated from growth (μ) and grazing (m) rates for total Chl*a* from dilution experiments and the following equations (Landry et al., 2000):

$$\text{PROD} = \mu \times C_o\ (e^{(\mu - m)t} - 1)/(\mu - m)t, \text{ and}$$

$$\text{MICRO GRAZ} = m \times C_o\ (e^{(\mu - m)t} - 1)/(\mu - m)t$$

where C_o is initial autotrophic biomass (mg C m^{-3}) and t = time (1 day). PROD and MICRO GRAZ estimates for the euphotic zone were determined by integrating individual rate estimates from the surface to the deepest incubation depth according to the trapezoidal rule.

2.6. Mesozooplankton biomass and grazing

Details of mesozooplankton biomass and grazing along 110°E are presented in Landry et al. (2020a). Briefly, the net tow samples were anesthetized with CO_2 (ice-cold soda water) and a sea-ice ice slurry (−1.8 °C), split into two ¼ sample fractions with a Folsom plankton splitter, and separately wet sieved through Nitex screens to produce two sets of 5 size classes: 0.2–0.5, 0.5–1, 1–2, 2–5 and >5 mm (the remaining ½ sample was formaldehyde preserved). One size-fractioned set was oven dried on pre-weighed Nitex filters, reweighed for dry weight (DW), then ground to a powder and subsampled for analyses of C:DW and N:DW contents on a Perkin Elmer CHN analyzer. Mesozooplankton biomass (C m^{-2}) was calculated from the sum of size-fractioned samples, the tow depths and the tow distances assuming 100% net capture efficiency. We averaged day and night tows for station mean biomass.

The second size-fraction set was analyzed on shipboard by the gut fluorescence method (Mackas and Bohrer, 1976). Samples were homogenized with 7 mL of 90% acetone in an ice bath with a Vibracell sonicator probe, extracted overnight at −20 °C and warmed to room temperature prior to analysis. The homogenate was shaken and centrifuged to remove particulates, and Chl*a* and phaeopigment (Phaeo) concentrations were measured by the acidification method using a 10AU fluorometer (Strickland and Parsons, 1972). We estimated grazing rates (G, mg pigment m^{-2} $time^{-1}$) as G = GPC * K, where GPC is the gut Phaeo content and K (min^{-1}) = 0.0026 (T°C) + 0.012 is the gut evacuation rate constant from Irigoien (1998). Mesozooplankton grazing impact on the phytoplankton community m^{-2} was calculated from the percent of water-column Chl*a* consumed d^{-1} integrated to the tow depth and averaged for day and night tows. C-based grazing estimates (MESO GRAZ below) were computed from EZ-integrated mean estimates of phytoplankton C:Chl*a*.

3. Results

3.1. Environmental conditions

Temperature and salinity define two major water masses along the 110°E transect (Fig. 1b and c). The high-salinity surface water (>35.7 psμ) between ~27.5 and 35°S is a distinctive feature of the southern IO subtropical region that sinks below lower density water to the north (Rochford, 1969; Woo and Pattiaratchi, 2008). We refer to this as subtropical water (STW; Wyrtki, 1973). The high-temperature, low-salinity water mass north of 14°S enters the Indian Ocean from the Pacific via the ITF and is referred to here as Indonesian Throughflow Water (ITW; Talley, 1995). Between STW and ITW is a zone (15.5–26°S) of high eddy activity and mixing with intermediate T-S properties and a subsurface salinity maximum between 150 and 250 m. South of the STW (>36°S) is the subtropical front where colder, lower-salinity subantarctic water converges with and subducts under the subtropical water mass.

Nitrate + nitrite and fluorescence sections show a generally positive relationship over the transect (Fig. 1d and e). Fluorescence is highest, 0.5–0.6 mg Chl*a* m^{-3}, in surface water of the subtropical front where nitrate + nitrite concentrations are elevated. Deep Chlorophyll Maxima (DCM) are mainly evident in the northern half of the transect where significant concentrations of nitrate + nitrite penetrate into the upper 100 m. The DCM is very faint or absent in the STW region, where mixed-layer depth (MLD, Fig. 1d) is deepest along the transect, though not intersecting the nitracline, as it does in the ITW region. MLD shallows to <50 m though most of the mixing region between STW and ITW (Fig. 1d).

The euphotic zone (EZ), here defined by the depth of penetration of 1% incident PAR, varied from 66 to 108 m and averaged 86 ± 12 m for the transect (Fig. 1e). Temperature profiles for the light depths sampled for community analyses and experimental incubations show relatively well-mixed conditions for the EZs overall, but the deeper sampling depths (1.5–2.5% I_o) enter the upper thermocline at some stations in the northern half of the transect (Fig. 2a). This is especially evident in the nitrate + nitrite profiles at 11.5, 12.5, 18.5 and 21.5°S (Fig. 2b), which show substantial concentrations of 1–8 μM in the lower EZ. Except for

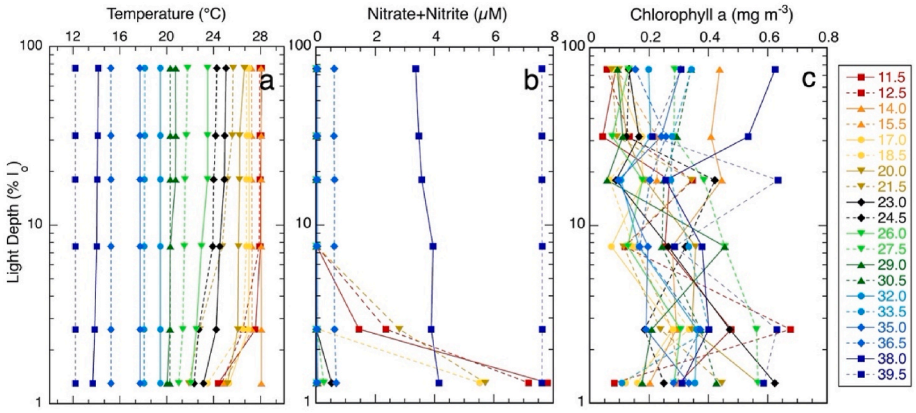

Fig. 2. Station profiles of Temperature (°C), Nitrate + Nitrite concentration (μM) and extracted Chl*a* (mg m^{-3}) from the CTD water samples collected at six light depths (% I_o) along 110°E. Station locations (Latitude, °S) are indicated in the color-coded legend.

stations in the subtropical front (36.5–39.5°S), nitrate + nitrite concentrations are extremely low (mean ± SEM, 0.024 ± 0.002 μM) at most stations down to the 7.6% I_o light depth (Landry et al., 2022). Conversely, silicate (not shown) was most depleted (0.4–0.7 μM) throughout the EZ at the subtropical front stations, while upper EZ concentrations generally exceeded 2 μM at all stations north of 32°S (range 1.7–2.7 μM; Landry et al., 2022). Phosphate concentrations exceeded nitrate + nitrite in the upper EZ at all stations north of 35°S (range 0.03–0.07 μM; Landry et al., 2022).

Although the ranges are similar (0.06–0.60 mg Chl*a* m^{-3}), the extracted Chl*a* concentrations from small discrete samples are more variable than suggested by the smooth CTD fluorescence profiles (Fig. 2c). For all but two stations (14 and 38°S), surface concentrations are <0.4 mg Chl*a* m^{-3}.

The environmental conditions experienced by the microbial community during incubation experiments differ in some ways from the conditions in the ambient water column. Consistent with the deeply mixed thermal structure, daily-averaged wind speeds were relatively strong, averaging 27 ± 2 km h^{-1} for the transect (range 12–45 km h^{-1}; Table 1). The freely mixed communities in the water column on the day preceding sampling experienced the strong south-to-north conditions of increasing temperature (Fig. 2a) and incident PAR, ranging from 5 to 37 E m^{-2} d^{-1} (Table 1). Bottle-contained communities in the experiments were in incubator boxes at constant relative percentages of incident PAR and also, due to transits between stations, experienced the sea surface temperature and PAR at 1.5° lower latitude stations during the following day. The differences between ambient and experimental temperatures vary from 0 to 2.8 °C, averaging +0.84 ± 0.15 °C, with larger differences at the southern end of the transect with the strongest latitudinal gradient in temperature. For PAR, significant (1.5X) differences between prior ambient light history and experimental conditions are mainly seen at scattered stations, with substantially higher incubation PAR at 36.5 and 27.5 °S and substantially lower incubation PAR at 38 and 11.5 °S (Table 1).

3.2. Chlorophyll and carbon biomass relationships

Population red fluorescence from FCM (cell abundance x mean RF $cell^{-1}$) is strongly correlated to Chl*a* concentrations from the HPLC pigment analyses (Fig. 3). For PRO, RF is related to divinyl Chl*a* (DVChl*a*) by the equation: RF $L^{-1} = 10^6 * (0.026 + 2.43 * \text{DVChl}a\ L^{-1})$ with $R^2 = 0.56$, $p < 10^{-6}$. For the combined populations of PRO, SYN and EUK, RF $L^{-1} = 10^6 * (-0.011 + 3.11 * \text{TChl}a\ L^{-1})$ with $R^2 = 0.72$, $p < 10^{-6}$. While slopes of the two relationships have overlapping 95% confidence limits, they do differ significantly ($p < 0.007$), suggesting that the different populations are not identical in cellular RF properties.

We applied the mean (±SEM) value from 120 paired comparisons of PRO red fluorescence to DVChl*a* (1 unit RF = 0.432 ± 0.011 fg Chl*a*) to all FCM populations to estimate their respective contributions to EZ-integrated Chl*a* at each station (Fig. 4a and b). Integrated Chl*a* in PRO increases through the subtropical front and STW (39.5–29°S) from ~7 to 50% of the total, remains a fairly constant 50–60% of the total through the mixing region, and declines in ITW at stations (12.5–14°S), where SYN increases. SYN Chl*a* is notably higher in the subtropical front and ITW areas and lowest in the mixing region. EUK accounts for the majority of Chl*a* at stations south of 32°S and a relatively consistent ~40%

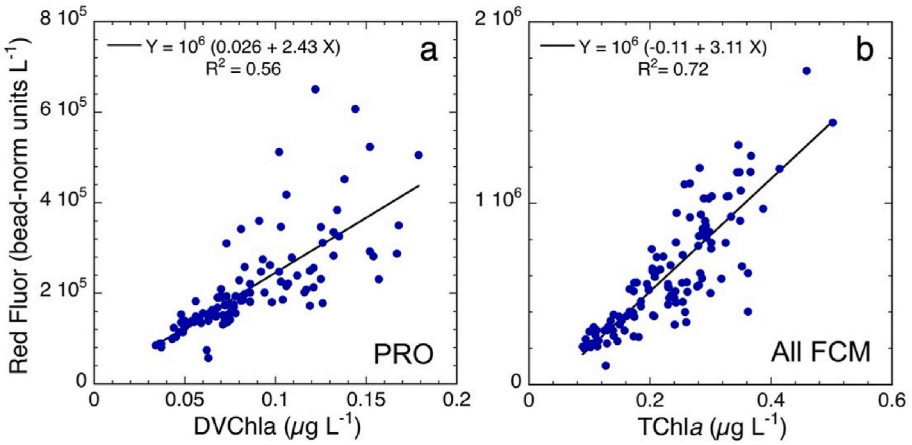

Fig. 3. Relationships between bead-normalized red fluorescence from flow cytometry and measured values of chlorophyll *a* from high-pressure liquid chromatography (HPLC). Data are all euphotic zone samples collected on evening CTD hydrocasts on the 110°E transect. a) Population red fluorescence for *Prochlorococcus* (PRO, cell abundance x mean cell fluorescence) relative to divinyl Chl*a* (DVChl*a*, μg L^{-1}). b) Total red fluorescence for *Prochlorococcus*, *Synechococcus* and photosynthetic eukaryotes (sum of population abundances x mean cell fluorescence) relative to Total Chl*a* (TChl*a*, μg L^{-1}).

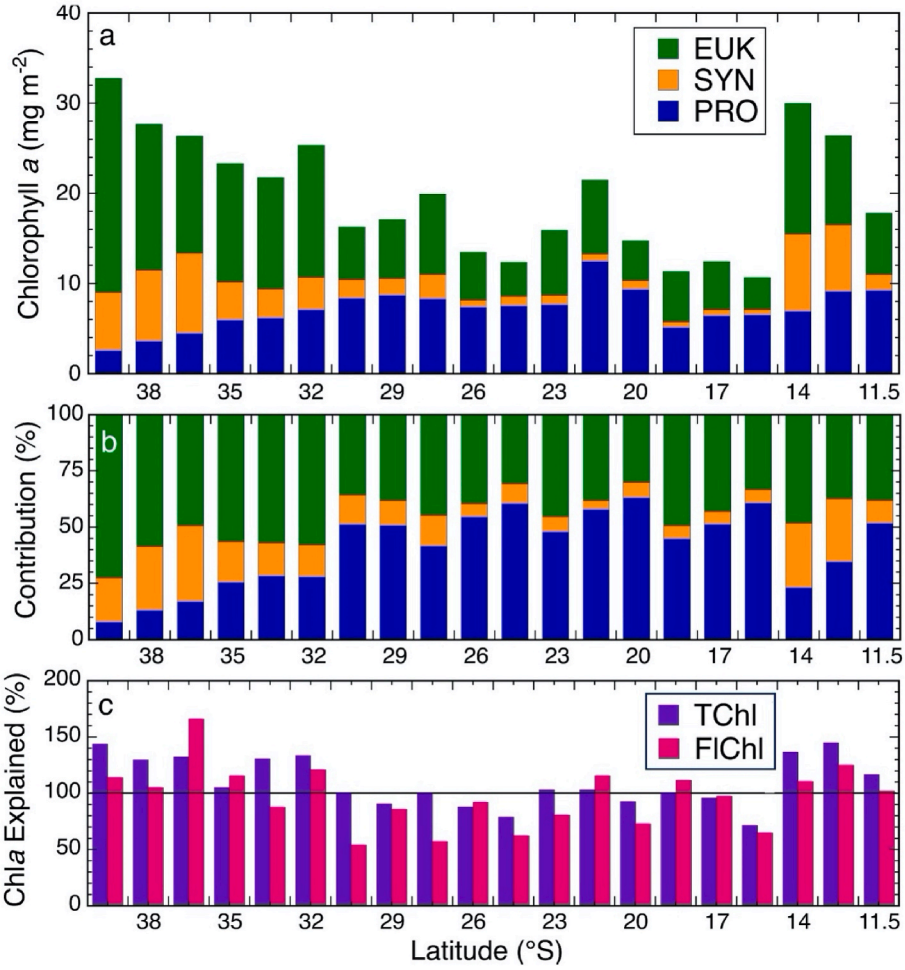

Fig. 4. Euphotic-zone (EZ) integrated estimates of chlorophyll *a* contained in *Prochlorococcus* (PRO), *Synechococcus* (SYN) and photosynthetic eukaryotes (EUK) along the 110°E transect. a) Chl*a* concentrations (mg m^{-2}) based on flow cytometric measurements of bead-normalized red fluorescence. b) Percent contributions (%) of population Chl*a* based on bead-normalized red fluorescence. c) Percent of Chl*a* explained by total red fluorescence relative to EZ-integrated Chl*a* from HPLC (TChl) and fluorometric (FlChl) analyses.

of Chl*a* through the central and northern transect.

In comparing the values of integrated Chl*a* from FCM red fluorescence to the station estimates from HPLC (TChl) and fluorometric (FlChl) measurements (Fig. 4c), we observe that RF estimates are closest to FlChl at the southern (32–39.5°S) and northern (11.5–14°S) ends of the transect, while RF corresponds better to TChl for the middle stations. Reasons for these differences are considered in Discussion section 4.1. Here, we note only that in the absence of clear offsets between RF-based estimates and measured Chl*a* for the transect as a whole, the FCM-measured populations appear to provide a reasonable representation of the total phytoplankton community.

Carbon biomass profiles based on FCM population abundances and

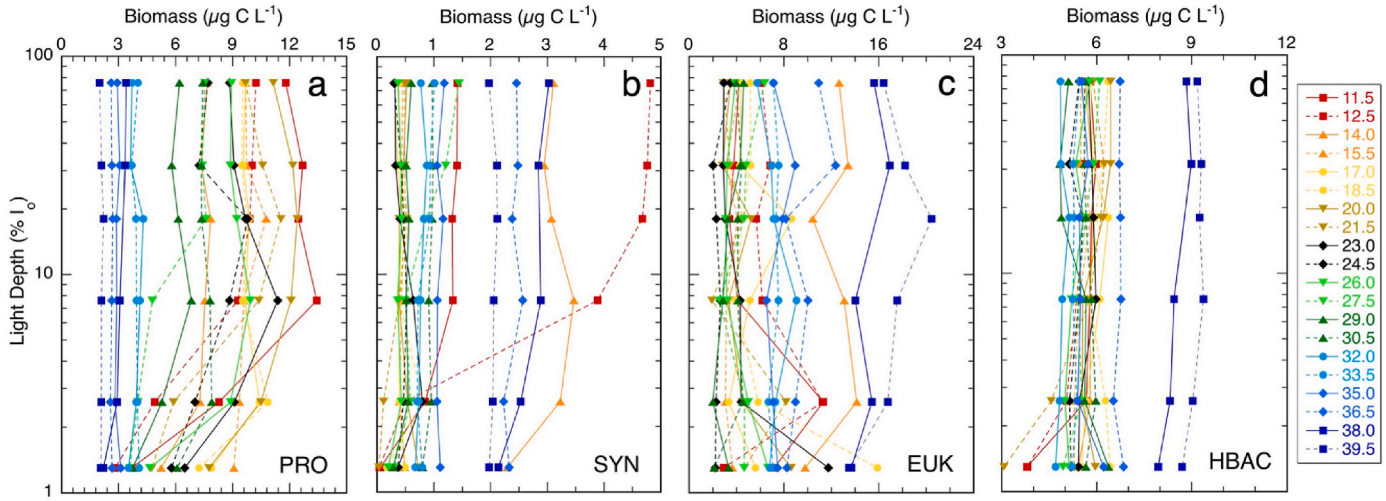

Fig. 5. Biomass profiles for flow cytometry populations at sampled light depths (% I_o) along the 110°E transect. PRO = *Prochlorococcus*; SYN = *Synechococcus*; EUK = photosynthetic eukaryotes; HBAC = heterotrophic bacteria. Station locations (Latitude, °S) are indicated in the color-coded legend. Profiles exclude data from one sample at 18% I_0 at 38°S for which all populations were anomalously low by a factor of 2, suggesting either a premature bottle trip or machine measurement error.

FALS-ratio sizing are presented by station in Fig. 5. PRO biomass ranges from ~2 to 12 μg C L^{-1} over the transect, increasing generally from south to north (Fig. 5a). SYN biomass exceeds 2 μg C L^{-1} only at the southern and northern ends of the transect; biomass declines progressively to minimum levels of 0.3–0.6 μg C L^{-1} in the STW and mixing regions and rises to the highest levels 3–4.8 μg C L^{-1} at ITW stations 12.5–14°S (Fig. 5b). EUK and HBAC both have their highest biomass values (16–20 and ~9 μg C L^{-1}, respectively) in the subtropical front (38–39.5°S) (Fig. 5c and d). EUK biomass declines to 3–5 μg C L^{-1} through the STW and mixing regions and is only high again in the ITW at 14°S. (Fig. 5c). HBAC biomass ranges narrowly from 5 to 7 μg C L^{-1} throughout the STW, ITW and mixing regions. EUK is the only FCM-distinguished group with clear and significant deep maxima in C biomass, occurring at the same locations where the upper nitracline intrudes into the base of the euphotic zone (11.5, 12.5, 18.5, 21.5 and 23°S; Fig. 2b,e and 5c).

C:Chl*a* ratios for the individual and combined FCM populations show roughly similar patterns but some variability in ranges (Fig. 6). Near-surface samples for all populations have minimum C:Chl*a* ratios, ~20–40 μg C (μg Chl*a*)$^{-1}$, in the nitrogen-rich subtropical front and highest ratios, 100–180 μg C (μg Chl*a*)$^{-1}$, at 11.5 or 14–18.5°S. The range of variability narrows in the deep EZ, approaching the minimum surface values observed at the subtropical front (Fig. 6).

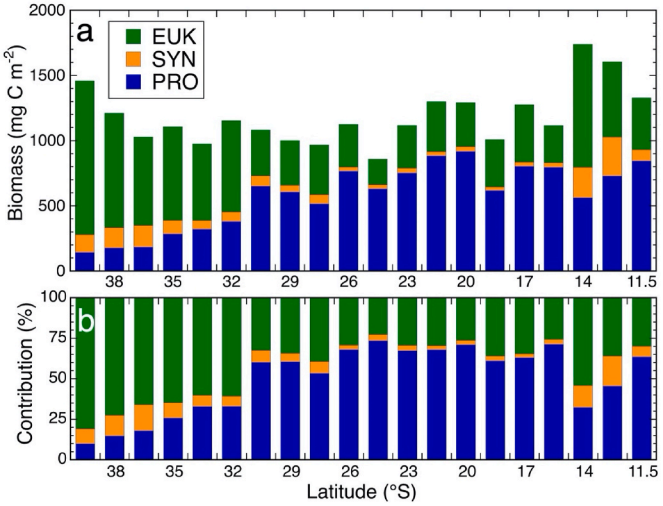

Fig. 7. Euphotic-zone integrated estimates of carbon biomass for *Prochlorococcus* (PRO), *Synechococcus* (SYN) and photosynthetic eukaryotes (EUK) along the 110°E transect. a) Carbon biomass (mg C m^{-2}) based on flow cytometric measurements of population abundances and mean cell carbon contents. b) Percent Contributions (%) of populations to total carbon biomass.

3.3. Integrated carbon biomass for the euphotic zone

In absolute terms, EZ-integrated biomass of PRO increases more-or-less linearly by 6.5 fold from 141 mg C m^{-2} at 39.5°S to 915 mg C m^{-2} at 20°S, and thereafter averages 700 mg C m^{-2} at lower latitudes (Fig. 7a). However, high percent contributions of PRO to phytoplankton C biomass (66.1 ± 2.1%, n = 9) occur throughout the broader mixing region (15.5–27.7 °S) between STW and ITW (Fig. 7b). Opposite to the latitudinal trends for PRO, both SYN and EUK have higher integrated C biomass and % contributions in the southern and northern ends of the transect and make their lowest contributions to community C biomass (3.6 ± 0.5 and 30.5 ± 1.8%, respectively) in the region between 15.5 and 27.7 °S. Despite these substantial shifts in phytoplankton biomass contributions along the 110°E transect, total integrated C varies only by a factor of two (860–1740 mg C m^{-2}; Fig. 7a). Seventeen of 20 stations exceed 1000 mg C m^{-2}, and the transect average is 1187 ± 50 mg C m^{-2}.

Consistent with the low variability in HBAC biomass profiles (Fig. 5d), integrated estimates of HBAC biomass are relatively uniform over the transect (Fig. 8a). Aside from the highest value of 616 mg C m^{-2} at 39.5°S, all other stations fall within 391–542 mg C m^{-2}, giving a transect average of 476 ± 11 mg C m^{-2}. In contrast, C biomass of mesozooplankton (MESO) exhibits a strong latitudinal trend, with lowest values (131–133 mg C m^{-2}) in the south at 32°S and 35–38°S and highest values (426–488 mg C m^{-2}) in the ITW at 11.5–14°S (Fig. 8c). Within the ITW region, MESO biomass parallels station variability in total phytoplankton biomass, averaging 29 ± 1% of the phytoplankton total. The MESO:PHYTO biomass relationship is lower on average (22 ± 2%) and more variable (11–37%) for the remaining 17 stations.

The EZ-extrapolated biomass estimates for ciliates and dinoflagellates from microscopical analyses (Fig. 8b) provide a crude approximation of the biomass of larger (>5 μm) protists that contribute to grazing, assuming that all dinoflagellates are functionally mixotrophic. The combined sample analyzed for 27.5°S had an anomalously high biomass of *Tripos* spp. that was unlikely to be representative of the EZ as a whole but clearly indicates the potential for enhanced

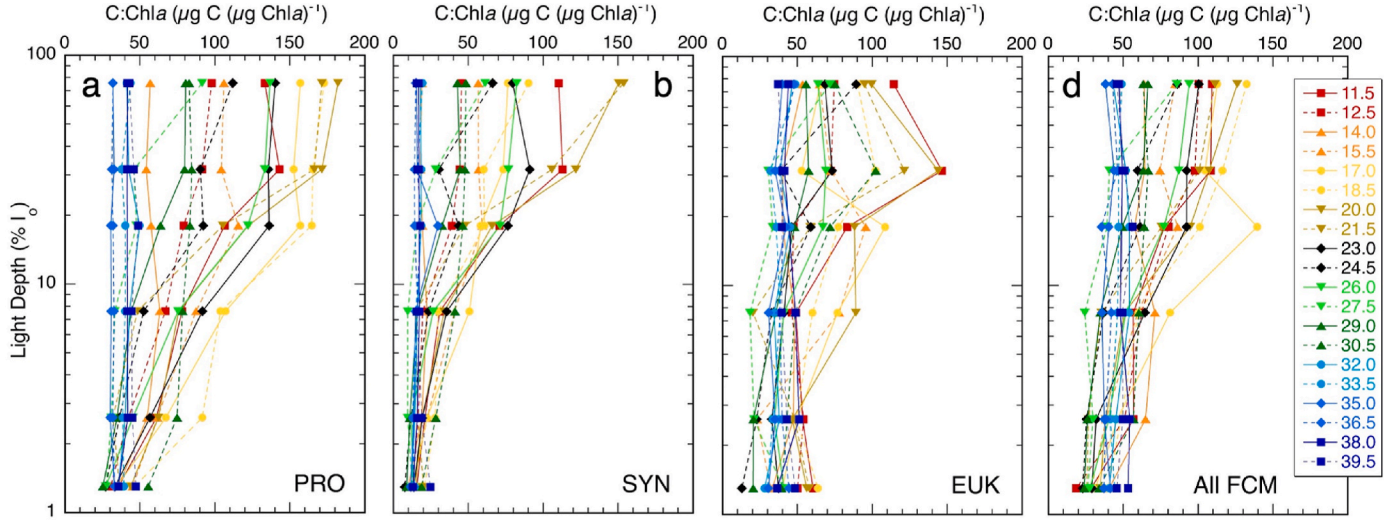

Fig. 6. Carbon:chlorophyll (C:Chl*a*) profiles for flow cytometry populations at sampled light depths (% I_o) along the 110°E transect. PRO = *Prochlorococcus*; SYN = *Synechococcus*; EUK = photosynthetic eukaryotes; All FCM = combined PRO, SYN and EUK populations. Station locations (Latitude, °S) are indicated in the color-coded legend. Profiles exclude data from one sample at 18% I_0 at 38°S for which all populations were anomalously low by a factor of 2.

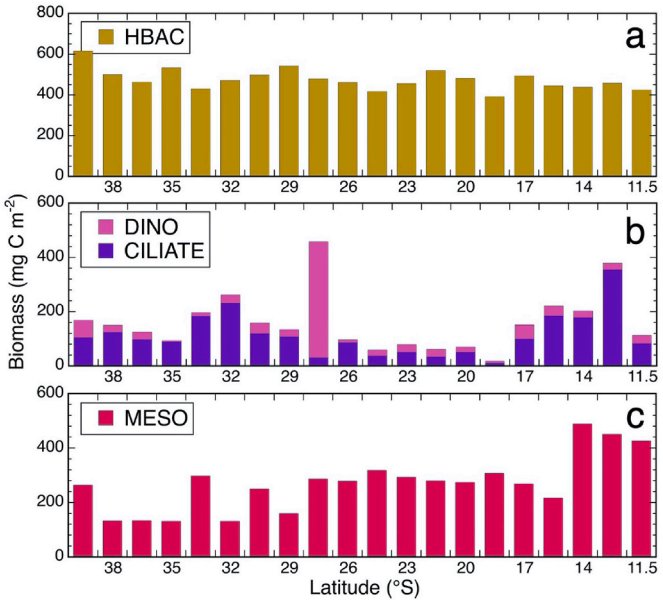

Fig. 8. Euphotic-zone (EZ) integrated estimates of carbon biomass for heterotrophic bacteria (HBAC), dinoflagellates (DINO), ciliates (CILIATE) and mesozooplankton (MESO) along the 110°E transect. a) HBAC biomass is based on flow cytometric measurements of population abundances and mean cell carbon. b) DINO and CILIATE biomass based on microscopical estimates for the upper EZ extrapolated to the full EZ. c) MESO biomass is based on average measured C biomass in day and night net tows.

concentrations at small scales. Excluding only the *Tripos* spp. at this station, integrated C biomass for dinoflagellates ranges from 5 to 61 mg C m^{-2} and averages 28 ± 3 mg C m^{-2} for the transect. Diatoms (not shown) analyzed in the same samples ranged from 0.4 to 35 mg C m^{-2} and averaged 6 ± 2 mg C m^{-2}. Diatoms and dinoflagellates containing Chl*a* would also have been counted in the photosynthetic EUK category, so they are not in addition to the previously estimated phytoplankton total from the FCM analyses (Fig. 7). Even so, they together comprise <3% of the total biomass estimates, on average, and 6.6% of EUK biomass; thus, these large phytoplankters are a small fraction of the community overall.

Ciliate biomass ranges from 9 to 354 mg C m^{-2} and averages 112 ± 18 mg C m^{-2} for the transect. Excluding the anomalous *Tripos* spp. biomass at 27.5°S, ciliates account for the majority of biomass associated with larger protistan grazers at 19 of the 20 stations, and 75 ± 3% overall. In the southern portion of the transect, from the subtropical front through much of the core STW (29–39.5°S), the integrated biomasses for protistan grazers and MESO are of comparable magnitudes (161 ± 18 versus 187 ± 25 mg C m^{-2}, respectively). Protistan grazer biomass decreases to their lowest levels as MESO biomass increases in the mixing area between 18.5 and 26°S (64 ± 11 and 292 ± 7 mg C m^{-2}, respectively). Biomass of both protistan grazers and MESO are highest in the ITW, averaging 231 ± 78 and 455 ± 18 mg C m^{-2}, respectively, in waters from 11.5 to 14°S (Fig. 8b and c).

3.4. Rate estimates of microbial growth and microzooplankton grazing

In general, profiles from dilution incubations show low rates of population cell growth and microzooplankton grazing mortality in the subtropical front and the STW south of 32°S (Fig. 9). Rates tend to be

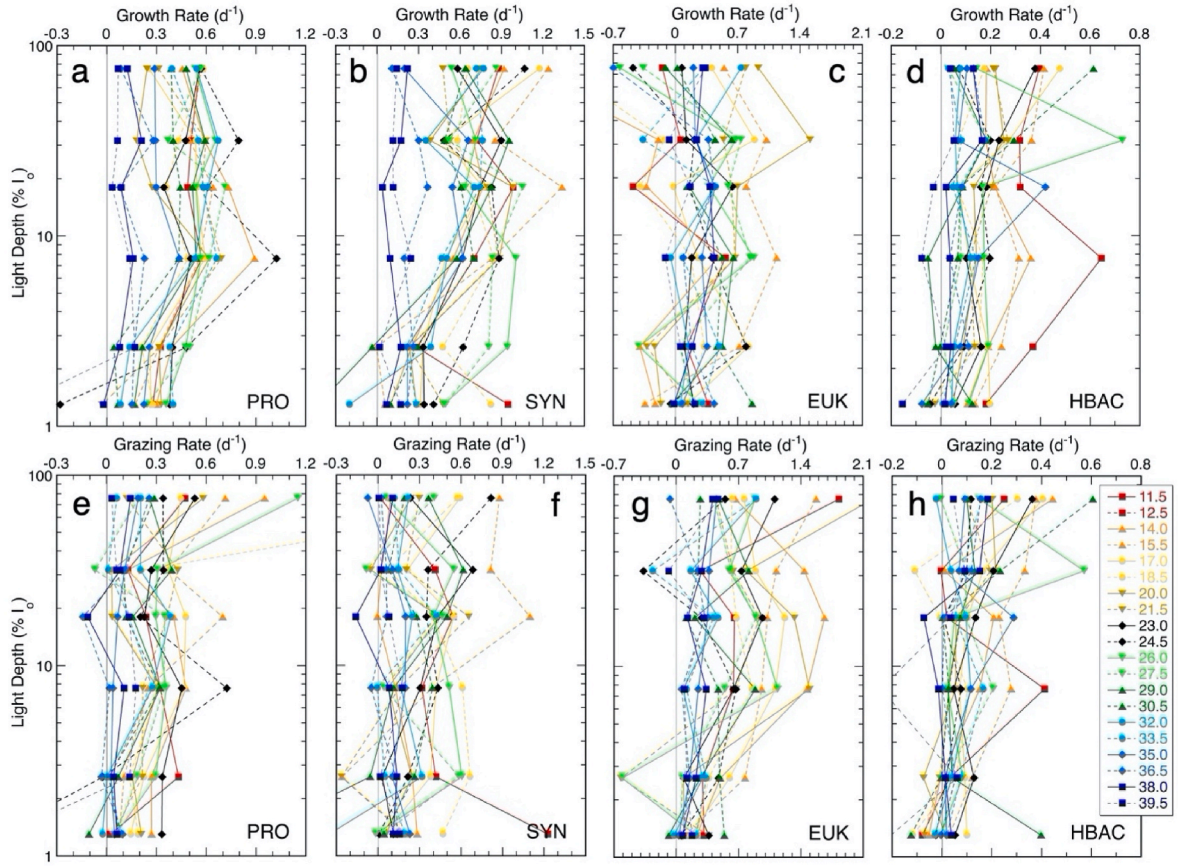

Fig. 9. Growth rates and microzooplankton grazing mortality for flow cytometry populations from dilution experiments incubated at euphotic-zone light depths (% I_o) along the 110°E transect. PRO = *Prochlorococcus*; SYN = *Synechococcus*; EUK = photosynthetic eukaryotes; HBAC = heterotrophic bacteria. Station locations (Latitude, °S) are indicated in the color-coded legend.

higher at the northern stations, but do not clearly line up with the south-to-north trends in latitudinal temperature and light (PAR). For PRO, most upper-EZ growth rate estimates north of the subtropical front lie between 0.3 and 0.6 d^{-1}, without a latitudinal trend (Fig. 9a). Grazing estimates are generally 0.2–0.5 d^{-1}, with occasional surface estimates of 0.7–1.2 d^{-1} (Fig. 9e). For SYN, upper-EZ growth rates lie between 0.5 and 0.9 d^{-1}, with grazing of 0.2–0.6 d^{-1} (Fig. 9b,f). EUK growth rates are mostly <0.8 d^{-1} and show high incidence of negative growth in the upper EZ at many stations, including in the ITW (Fig. 9c). In contrast, EUK grazing estimates are the most organized by latitude, with highest values (>1.2 d^{-1}) in waters north of 15.5°S (Fig. 9g). With few exceptions, growth and grazing rate estimates for HBAC are <0.4 d^{-1}, with the bulk 0.2 d^{-1} or lower (Fig. 9d,h).

Most growth rate estimates for the phytoplankton community based on Chl*a* vary between 0.2 and 1.0 d^{-1}, with some negative growth rates in the high-light surface incubations and subsurface maxima at some stations in the range of 1.2–1.6 d^{-1} (Fig. 10a). Microzooplankton grazing estimates are generally in a similar range, most <1.0 d^{-1} with scattered higher rates up to 1.7 d^{-1} (Fig. 10b). For both growth and grazing estimates, lower rates are concentrated in southern stations and higher rates are more evident in the northern transect (Fig. 10a and b).

3.5. EZ-integrated production and grazing

EZ estimates of phytoplankton carbon production (PROD), calculated from biomass and dilution rates, are compared to integrated C estimates of microzooplankton (MICRO) and mesozooplankton (MESO) grazing in Fig. 11. Based on the sums of FCM-measured populations, phytoplankton PROD ranges from 111 to 655 mg C m^{-2} d^{-1}, increasing relatively linearly from 39.5°S through the STW to 27.5°S before leveling off at northern stations (Fig. 11a). Mean total PROD is 466 ± 35 mg C m^{-2} d^{-1}. EUK accounts for most of the production south of 35°S, while PRO dominates at all other stations. SYN contributes most to PROD (14–33%) in the ITW region, although this includes one station (14°S) where integrated EUK PROD was a negative value, therefore underestimated, and set to zero for the PROD total. Grazing estimates based on the sum of MICRO GRAZ for FCM populations plus MESO GRAZ range from 131 to 1071 mg C m^{-2} d^{-1}, increasing generally from southern to northern stations and averaging 461 ± 54 mg C m^{-2} d^{-1} over the transect. MICRO dominates grazing, accounting for 85 ± 2% on average (range 64–95%).

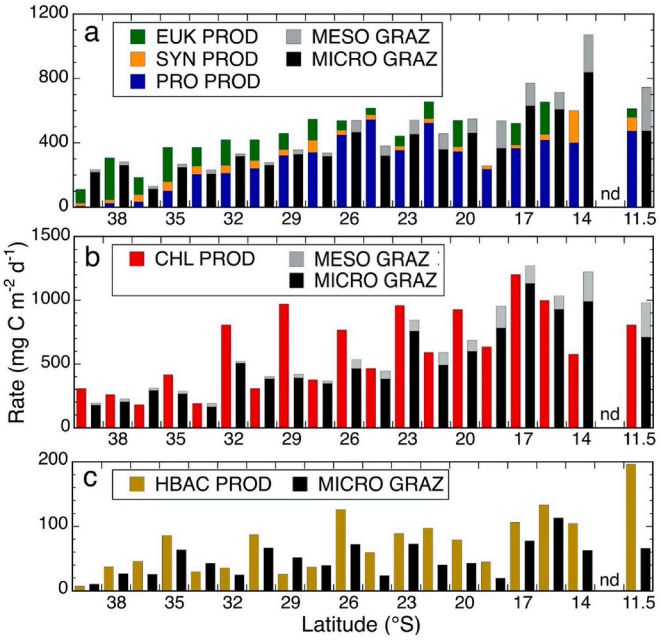

Fig. 11. Integrated euphotic-zone (EZ) estimates of carbon production (PROD) and grazing (GRAZ) rates along the 110°E transect. a) PROD and microzooplankton grazing (MICRO GRAZ) rates (mg C m^{-2}) based on flow cytometric populations *Prochlorococcus* (PRO), *Synechococcus* (SYN) and photosynthetic eukaryotes (EUK). b) PROD and MICRO GRAZ rates (mg C m^{-2}) from dilution experiments based on Chl*a*. MESO GRAZ based on the fraction of Chl*a* removed by mesozooplankton d^{-1} and integrated values of C:Chl*a*. c) PROD and MICRO GRAZ of heterotrophic bacteria (HBAC).

Phytoplankton community estimates of PROD based on Chl*a* range from 182 to 1202 mg C m^{-2} d^{-1} and average 618 ± 72 mg C m^{-2} d^{-1} (Fig. 11b). Station PROD estimates are more irregular than for the sum of FCM populations, but the general trend is similar with a south-to-north increase leveling off or declining slightly at lower latitudes. Chl*a*-based GRAZ estimates vary from 195 to 1272 mg C m^{-2} d^{-1}, with a transect mean rate of 604 ± 80 mg C m^{-2} d^{-1}. MICRO accounts for 89 ±

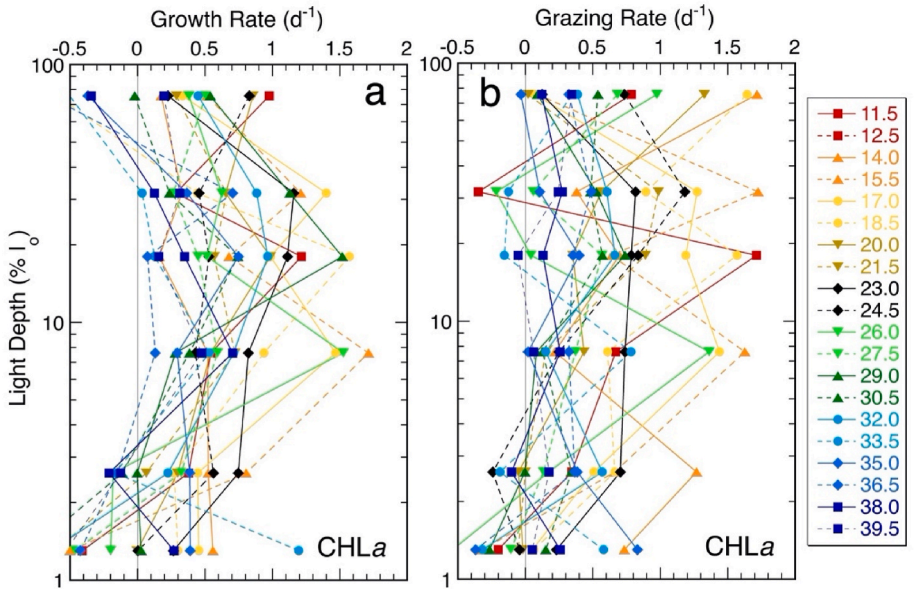

Fig. 10. Chlorophyll-based growth rates (a) and microzooplankton grazing (b) from dilution experiments incubated at euphotic-zone light depths (% I_o) along the 110°E transect. Station locations (Latitude, °S) are indicated in color-coded legend.

2% of total GRAZ on average (range 72–97%).

Integrated estimates of HBAC PROD are approximately an order of magnitude lower than for phytoplankton and show a general increasing trend from high-to-low latitude with substantial variability between stations (Fig. 11c). HBAC PROD and MICRO GRAZ range from 7 to 196 and from 10 to 113 mg C m^{-2} d^{-1}, respectively, with transect averages of 75 ± 47 and 50 ± 26 mg C m^{-2} d^{-1}.

Although the carbon-based rate estimates from FCM populations are ~25% lower on average compared to estimates from Chl*a*, both show strong relationships ($p < 10^{-8}$) between PROD and GRAZ (Fig. 12a). Slopes for the two relationships are not statistically significant ($p > 0.35$), and confidence limits (95%) for both regressions broadly overlap with each other and with the 1:1 line (FCM = 0.79–1.22; Chl*a* = 0.77–1.12). Thus, both relationships indicate that a general balance of phytoplankton production and grazing processes extended over the 110°E transect during the period of our investigation. For HBAC, MICRO GRAZ averages ~0.6 * PROD rates, with 95% confidence limits of 0.48–0.72 (Fig. 12b).

4. Discussion

We used complementary methods of flow cytometry, pigment analyses, microscopy, zooplankton net sampling and experimental incubations to constrain estimates of microbial community biomass, C:Chl*a* ratios, growth rates, production and grazing impacts from micro- and mesozooplankton across the varying water masses of the 110°E transect. For the austral late-autumn (May–June) period of our investigation, 110°E waters north of the subtropical front were generally oligotrophic and picophytoplankton dominated, but with substantial south-to-north gradients in incident light and temperature. These gradients in environmental growth conditions mainly manifest in increased biomass turnover, measured as carbon-based production and grazing rates, while integrated biomass of phytoplankton and heterotrophic bacteria show no consistent trends with latitude. Phytoplankton production and grazing processes are tightly coupled over the gradient, and biomass accumulates in the higher levels of the food web (mesozooplankton) at lower latitudes. In the subsections below, we first consider methodological factors that might influence interpretations of the study results. We then put our findings in the context of previous results for the eastern Indian Ocean and other open-ocean low-latitude ecosystems.

4.1. Methodological considerations and interpretations

Flow cytometric analyses of cell abundances, fluorescence and light scatter tie together the pigment, biomass and rate components of our study. Where the relationships can be validated, for example, between FCM red fluorescence (RF) and measured Chl*a* (Fig. 3a and b), reasonable agreement is evident. Nonetheless, substantial differences are seen between EZ-integrated RF and TChl*a* in some locations, notably at the southern and northern ends of the transect (Fig. 4c). Among possible explanations, the fact that FCM and HPLC pigment samples are taken from different bottles and depths on the same hydrocast certainly contributes to the variability in comparing individual samples. We expect that FCM subsamples drawn directly from the HPLC water samples would have had lower scatter and higher correlation coefficients than in Fig. 3, though not necessarily different depth-integrated estimates based on multiple analyses per profile in Fig. 4. For the stations at 11.5 and 12.5°S, however, FCM sampling hit the well-developed DCM peaks whereas the interpolated values from TChl*a* samples missed the DCM. At these stations, therefore, the discrepancies are at least partially explained by sampling underestimates of TChl*a*.

In general, systematic bias can arise where rare large cells exert a disproportionate effect on the mean values of RF (or FALS) in the FCM analyses, which are then applied to all cells in the population. Such circumstances (greater frequency of larger cells) are expected in the southern and northern ends of the transect where nutrient concentrations are higher or the upper nitracline enters the EZ (Fig. 1d and e and 2), and where we observe the largest discrepancies. RF underestimates of TChl*a*, such as those observed at 15.5 and 25.5°S, might also occur where a significant fraction of cells does not survive the preservation, freezing and thawing steps prior to FCM analyses. That might depend on specific taxa or environmental circumstances, however, because, aside from these stations, there is little evidence that we are missing a significant portion of the Chl*a*-containing community. Overall, we attribute most of the discrepancies between RF-based Chl*a* estimates and TChl*a* to the EUK component, which are the more fragile, taxonomically diverse, size-variable and least abundant (least precisely enumerated) cells in the analysis, compared to PRO and SYN.

Our assignments of base values for cell C contents of the FCM-distinguished populations were based on well-used relationships and size scaling but are arbitrary to the extent that different choices would have led to different group contributions to community biomass estimates (Figs. 5 and 7) and different C:Chl*a* values (Fig. 6). Past estimates of C contents range from 15 to 250 fg C $cell^{-1}$ for PRO (Moore, 1997; Shalapyonok et al., 2000), 40 to 434 fg C $cell^{-1}$ for SYN (Heldal et al., 2003; Casey et al., 2013); 162 to 3980 fg C $cell^{-1}$ for EUK (Fuhrman et al., 1989; Worden et al., 2004), and 7.5 to 30 fg C $cell^{-1}$ for HBAC (Fukuda et al., 1998; Pomroy and Joint, 1999). Our base values of 32 and 11 fg C $cell^{-1}$ for PRO and HBAC, respectively, are based on cell biovolume measurements for open-ocean waters of the Arabian Sea. Our base values for PRO, SYN (155 fg C $cell^{-1}$) and EUK (3150 fg C $cell^{-1}$) also fall within the calibrated cell estimates of Casey et al. (2013) for PRO and SYN in upper EZ waters during summer stratified months

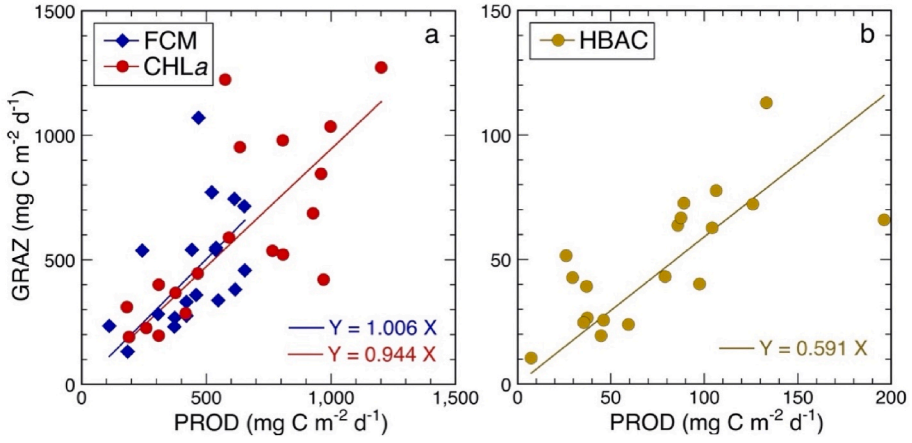

Fig. 12. Relationships between euphotic-zone integrated estimates of phytoplankton production (PROD) and grazing (GRAZ) for phytoplankton and heterotrophic bacteria (HBAC) along the 110°E transect. a) Blue diamond (FCM) symbols are from combined flow cytometry populations (PRO, SYN and EUK) from Figure 11a; red circles (CHL) are Chl*a* from Figure 11b, and GRAZ is combined micro- and mesozooplankton grazing (MICRO + MESO) from Figure 11a,b. b) HBAC PROD and MICRO GRAZ from Fig. 11c. All regressions are forced through zero.

(August–October) in the Sargasso Sea, within the calibrated mean annual C estimates for EUK from the same region (Casey et al., 2013), and within the more typical cell C values used in many other studies (Ishizaka et al., 1994; Blanchot and Rodier, 1996; Zubkov et al., 2000; Claustre et al., 2002; Veldhuis and Kraay, 2004).

Relative FALS scaling of cell sizes, as opposed to using fixed cell C values, allows us to account for variability in cell size and biomass with depth and latitude. For the latter, we determined that mean cell C values for the upper EZ ranged from 29 to 39 fg C cell^{-1} for PRO and from 129 to 214 fg C cell^{-1} for SYN, both with declining south-to-north trends (Landry et al., 2022). HBAC ranged narrowly around 11 fg C cell^{-1} at all stations while upper EZ mean C for EUK varied from a minimum of ~2000 fg C cell^{-1} at 12.5–14°S to a maximum of 4200–4600 fg C cell^{-1} at 17–18°S. For depth variability, we found that cell size variability at individual stations was consistently low in the upper EZ above 7.6% Io, where the water column was well mixed (Landry et al., 2022). However, PRO and SYN cells in the deep EZ were significantly larger than surface cells (>12% and up to 150% greater C) at all stations north of 29°S, except 14 and 15.5°S. These coincide, for the most part, to stations where a DCM was evident (Fig. 1). HBAC did not show notable depth variability in cell C at any station, and EUK cells in the deep EZ were always similar to or up to 50% smaller than cell sizes of surface samples, whereas deeper PRO and SYN cells were larger than surface cells. Thus, in the absence of measurements for each population at each depth, there are no general corrections for depth or latitudinal variability that would be applicable to cell sizes of all populations.

The C:Chla profiles in Fig. 6 incorporate all of the measured cell variability in RF and FALS. Consequently, absolute values would change with different assumptions about base cell C estimates, but the relative station differences would remain robust. For cells experiencing consistently high PAR in the upper EZ (i.e., stations north of 26°S; Table 1), the variability in C:Chl*a* ratios can be reasonably viewed as relating to varying degrees of nutrient (N) limitation (Geider et al., 1997; Taylor et al., 1997). Adopting that interpretation here, the profiles from 20 to 21.5°S with the highest C:Chl*a* define the area of strongest nutrient limitation for all populations, with 17–18.5°S also high from PRO and 11.5°S high for SYN and EUK.

Individual rate estimates from dilution experiments (Figs. 9 and 10) come from paired unreplicated bottles, and thus incorporate random errors that are at least partially averaged out in the EZ-integrated rate estimates and latitudinal trends (Fig. 11). With regard to possible biases or artifacts, one concern is the timing of experiments, which were setup less-than-ideally in the evening when some populations undergo semi-synchronous cell division (Vaulot, 1992; Vaulot et al., 1995; Liu et al., 1998). Thus, growth rate estimates may have some carryover effect from the prior daylight period in addition to the light conditions experienced during the full day of incubation. Also, if incubation conditions delay or advance cell division cycles relative to those experienced in the water column, that could lead to under- or over-estimates of growth relative to grazing over the 24-h period. We note, for example, that cell growth rates and microzooplankton grazing estimates are not in perfect balance for bacterial populations, as they are in some studies (e.g., Landry et al., 2011; 2016b). For PRO and HBAC, the mean net growth rates over the integrated EZ are relatively small (0.06 ± 0.06 and 0.05 ± 0.02 d^{-1}, respectively) and might reasonably be explained by either direct or indirect impacts of the missing mesozooplankton predation in the incubation experiments. Direct mesozooplankton grazing on bacteria-sized particles is expected from appendicularians, which were abundant along the transect, comprising 11–23% of the mixed-layer zooplankton collected by a towed Continuous Plankton Recorder in water north of the subtropical front (Davies et al., this volume). Appendicularians also have substantially (up to 10X) higher clearance rates than suspension-feeding copepods of similar biomass (Alldredge, 1981). Based on measured clearance rates of *Oikopleura fusifomis* on bacteria in a subtropical estuary (Scheinberg et al., 2005), water-column densities of one appendicularian per 15–18 L would be sufficient to account fully for the grazing on PRO and HBAC not provided by microzooplankton. In addition, the absence of mesozooplankton predation on large microzooplankton (ciliates and large dinoflagellates) in the incubations can indirectly cascade to lower levels via elevated grazing on intermediate EUK-sized consumers, which reduces grazing on bacteria. First et al. (2009) observed, for example, that their results from size-fractioned dilution experiments in oligotrophic waters of the Gulf of Mexico could be reproduced by cascading trophic interactions in a model with three interacting consumers.

Compared to PRO and HBAC, the net rate differentials between growth and microzooplankton grazing for SYN and EUK are more substantial and in opposite directions (+0.31 ± 0.3 versus −0.29 ± 0.9 d^{-1}, respectively). For SYN, which contributes relatively little to total community production and grazing (Fig. 11), the large net growth discrepancy implies either that growth rates might be overestimated, possibly by an acceleration of cell division by experimental timing or incubation conditions, or that we are missing an important EZ loss term from the incubation bottles. SYN is notable among pico-phytoplankton in being strongly linked to export processes (Amacher et al., 2013; Guidi et al., 2016) as well as being resistant to digestion by metazoan consumers (Johnson et al., 1982; Pfannkuche and Lochte, 1993; Gorsky et al., 1999; Wilson and Steinberg, 2010; Stukel et al., 2013). Aggregate formation has been hypothesized as a mechanism that both facilitates SYN sinking as well as increases their availability to mesozooplankton grazers which concentrates undigested SYN into fast sinking pellets (Agustí et al., 2015; Deng et al., 2016; Stukel et al., 2013). Metagenomic studies have also demonstrated very substantial differences in export contributions of SYN clades compared to their relative abundances in the water column (e.g., De Martini et al., 2018; Valencia et al., 2021). Our observed decoupling of growth and microzooplankton grazing rates for SYN in incubation experiments might therefore be indicative of an outsized role of local strains in export, possibly combined with digestion resistance to grazing by some protists such that cells disappear from FCM analyses at a lower rate than they are actually consumed.

For EUK, the high growth rate variability and substantial negative rates found in locations with temperatures of 27–28 °C (Figs. 9 and 11a) are consistent with viral infection or spontaneous lysis, which have been reported more prevalent for picoeukaryotes than photosynthetic bacteria and exacerbated by high light and temperature (Agustí and Sánchez, 2002; Baudoux et al., 2007: 2008; Bidle, 2016). As noted by Landry et al. (2022), the declines in our experiments were not triggered by abrupt differences in light or temperature between collection and incubation days (Table 1), and they occurred in bottles that had not been screened, filtered or manipulated in any way other than gentle filling. However, the light conditions experienced by cells held at high light for the full photoperiod in deck incubators clearly differed from the average conditions experienced in a freely mixed water column, which may have led, for example, to weakened cells in the experiments more likely to lyse during sample preservation, freezing and thawing prior to FCM analysis. Thus, it is not clear whether EUK cells were lost during the incubation or in post-experiment handling. In this regard, it is tempting to consider the FCM-based analyses of production and grazing as likely more accurate that the Chl*a*-based estimates, because the former are based on relatively precise enumerations of individual cells while the latter have pigment corrections. Considering the issues on both sides, we view the FCM- and Chl*a*-based analyses as providing equally valid or flawed representations, as the case may be, of community growth and grazing rates. The power of combining these approaches in the present study is that they give mutually supportive trends and relationships.

4.2. Plankton dynamics of the eastern Indian Ocean

The historic IIOE sampling along 110°E in 1962–63 was the first integrated investigation of circulation, nutrients, primary productivity and zooplankton in the eastern Indian Ocean (Jitts, 1969; Humphrey and Kerr, 1969: Newell, 1969: Rochford, 1969, 1977; Tranter, 1977a,b;

Tranter and Kerr, 1969, 1977) and here provides the broader seasonal and spatial context for our May–June cruise results. According to Jitts (1969), May–June coincides with the seasonal transition to high primary production (beginning of the austral winter SE monsoon), which persists from mid-May to October in tropical waters north of 15°S but develops later and has shorter duration (mid-June through August) in subtropical waters at 30–32°S (IIOE sampling did not extend to the subtropical front). Part of the production gradient that we observe between southern and northern ends of the transect is therefore explained by the timing and sampling direction of the 2019 cruise, which began during a period of moderate primary production in the south and ended during the higher production season in the north. During the relevant time periods, the noon-to-sunset ^{14}C incubations of Jitts (1969) under simulated *in situ* light conditions averaged 69 mg C m^{-2} h^{-1} for <15°S stations and 24 mg C m^{-2} h^{-1} for 30–32°S, which correspond to daily rates of 828 and 288 mg C m^{-2} d^{-1}, respectively, assuming sustained rates over a 12-h photoperiod. These values are reasonably close to 24-h production estimates from the present experiments at latitudes <15.5°S (578 ± 56 and 793 ± 122 mg C m^{-2} d^{-1} for FCM and Chl*a*-based rates, respectively) but a little lower than our estimates for STW >30°S (388 ± 11 and 472 ± 128 mg C m^{-2} d^{-1}). Given that historical estimates of ^{14}C uptake often underestimate the rates from contemporary measurements by a factor of 2 or more (Marra and Heinemann, 1987), the good agreement here might be attributed to 110°E IIOE investigators being ahead of their time in recognizing and mitigating poisoning effects during seawater collection and using blue filters to simulate deep-EZ light conditions (Jitts, 1963, 1969). On the other hand, significant IIOE rate underestimates due to historical methodological issues could also be masking any evidence of diminished production over the past six decades. The available data does not allow us to distinguish between these alternatives.

IIOE sampling shows two seasonal peaks of mesozooplankton biomass, with May–June being a low period between them (Tranter and Kerr, 1969). The major zooplankton peak occurs in August–September (~2–4 X May–June biomass) during the late SE monsoon, and the minor peak occurs in February–March in the late phase of the austral summer NW monsoon. Despite the seasonal trends, the latitudinal gradient from low mesozooplankton biomass south of 26°S (STW) to high biomass north of 14°S (ITW) (Fig. 8c) remains a fairly consistent year-long feature of the study region (Tranter et al., 1977). However, the biomass structure also includes variability in the types and timing of macrozooplankton and micronekton, the presumptive predators of mesozooplankton sampled by large trawl nets, which in general lag the peak biomass of mesozooplankton by 2–3 months (Legand, 1969). Based on these IIOE timelines, we frame our cruise as capturing the onset of elevated primary productivity in tropical-subtropical waters associated with the SE monsoon, during which mesozooplankton biomass will accumulate to be eventually overtaken by a later peak of larger predators. For our most southern stations in the subtropical front that were not sampled during IIOE, our cruise clearly occurred during a period of seasonal cooling and deeper mixing when light, rather than nutrients, provides the major constraint on productivity and dilution decreases grazing (Sverdrup, 1953; Behrenfeld, 2010).

Recent studies in the eastern IO have focused on the impacts of mesoscale eddies on productivity, zooplankton and fishery recruitment (Strzelecki et al., 2007; Waite et al., 2007b, 2019; Wang et al., 2014; Säwström et al., 2014) or the Leeuwin Current region further to the east (Thompson et al., 2011; Lourey et al., 2013; Sutton and Beckley, 2016). The center areas of the anticyclonic warm-core eddies that form off western Australia are Leeuwin Current water, with the tropical signature of lower salinity as well as some coastal phytoplankton (diatom) influences (Feng et al., 2007; Paterson et al., 2007). In Waite et al. (2007a), two eddies sampled in the vicinity of 31–32°S, 110°E in October, the end of the SE monsoon, differed 2-fold in integrated ^{14}C primary production, with the warm-core eddy higher in productivity (400 versus 240 mg C m^{-2} d^{-1}) as well as zooplankton biomass (780 versus 390 mg C m^{-2}; Strzelecki et al., 2007) than the cold-core eddy. The production values fall within our 190–808 mg C m^{-2} d^{-1} estimates for integrated production in the 30.5–33.5°S region (Fig. 11), but our averages (404 ± 16 and 436 ± 189 mg C m^{-2} d^{-1} for FCM and Chl*a*, respectively) are closer to the higher warm-core eddy rates. Our zooplankton biomass estimates in this latitudinal range (283 ± 12 mg C m^{-2}) are lower than both the warm- and cold-core eddy estimates of Strzelecki et al. (2007), which were sampled to a deeper (150 m) depth and later in the high production season when mesozooplankton biomass has accumulated and shifted to predominately carnivorous taxa (60–70% carnivores; Strzelecki et al., 2007).

To our knowledge, there are no previous grazing estimates for mesozooplankton along the 110°E transect, but microzooplankton grazing was measured in the eddy studies as well as at three stations across the Leeuwin Current (Paterson et al., 2007, 2008). Paterson et al. (2007) found that microzooplankton consumed all or most phytoplankton production in both eddy types, with large dinoflagellates the major grazers in the warm-core eddy while ciliates dominated in the cold-core eddy. In seasonal experiments conducted with surface water samples from a coastal lagoon to the continental slope, microzooplankton consumption generally balanced cell growth of FCM-measured picoplankton populations at all times and stations, while Chl*a*-based rates exhibited substantial positive net growth, though uncorrected for photoacclimation effects (Paterson et al., 2008). To the extent that comparisons can be made, these prior results are consistent with the present finding of a relatively close coupling of production and grazing processes, with the latter provided mainly by microzooplankton.

4.3. Comparisons to other subtropical and tropical ecosystems

In Table 2, we compare the ranges of measured EZ characteristics along the 110°E transect to those of other low-latitude, warm-water ecosystems that have been investigated by similar methods. Despite occupying a distinctly different latitudinal range, the 110°E stations compare particularly well to the equatorial Pacific in EZ depth, integrated TChl*a*, production and grazing. The microzooplankton biomass for 110°E is lower relative to other systems because heterotrophic flagellates (other than >5-μm dinoflagellates), often comprising half or more of that biomass, were not enumerated in the present study. The lower mesozooplankton biomass and grazing is explained by our sampling during the 110°E seasonal mesozooplankton minimum. The equatorial Pacific upwelling system is a meaningful basis of comparison to the present results because an inverse network model for that region incorporating mean values and uncertainties for experimental rate profiles was consistent with many of the system's independently measured parameters and fully explained how trophic flows originating from small phytoplankton and microzooplankton-dominated grazing supported high growth rates of mesozooplankton (Landry et al., 2020b). While such an analysis is beyond the scope of the present study, it is reasonable to expect that similar trophic interactions might also apply in the eastern IO. There are, however, substantial differences between the two regions in the structure and composition of the phytoplankton communities. Notably, flagellates have a major role in the equatorial Pacific, with PRO and diatoms making lesser and approximately equal (18%) contributions to production (Landry et al., 2011).

New production in the equatorial Pacific derives from Trade Wind divergent upwelling on the equator, while the ITF is a major source of new nutrients to the eastern IO (Ayers et al., 2014), which shifts the location of nutrient-enhanced tropical waters substantially to the south. In addition, strong wind-driven upwelling along the southern coast of Indonesia during the SE monsoon forms a prominent thermocline dome (Java Dome) where the westward flowing South Equatorial Current takes an anticyclonic turn (Wyrtki, 1962). The original 110°E IIOE investigations extended to 9.5°S, approximately a degree south of the Java Dome upwelling. The seasonal mesozooplankton biomass maximum there is 5200 mg C m^{-2} during the SE monsoon (July and August), based

Table 2
Comparisons of biomass, production and grazing rates measured along 110°E in May–June 2019 to measurements from open-ocean studies in the Arabian Sea, Gulf of Mexico, equatorial Pacific and eastern tropical Pacific (Costa Rica Dome). ML = Mixed Layer; EZ = Euphotic Zone; TChl*a* = Total chlorophyll *a* (HPLC). All measurements integrated to EZ depth defined by penetration of 1% Io.

Variable	East IO 110°E[1]	Arabian Sea[2]	Gulf of Mexico[3]	Equatorial Pacific[4]	East Trop Pacific[5]
Profiles (n)	19	27	11	30	16
Latitude	11.5–39.5 °S	10-23 °N	25-28 °N	4°S-4°N	6-11 °N
ML Temp (°C)	12–28	20–29	24–27	24–27	26–29
1% EZ Depth (m)	66–108	42–131	80–115	66–108	42–59
TChl*a* (mg m^{-2})	11–23	18–124	8–14	12–28	6–43
Biomass (mg C m^{-2})					
Phototrophs	967–1604	720–2890	849–1688	594–1766	828–2424
H-Bacteria	391–616	510–1740	414–722	180–738	189–622
Microzoo	18 - 379*	320–1350	146–724	233–870	145–479
Mesozoo	131–488	360–5016	89–864	268–1580	580–6900
Rate (mg C m^{-2} d^{-1})					
Phyto PROD	111–1201	600–2420	184–652	268–1426	291–1592
Microzoo GRAZ	113–1131	258–1999	48–499	248–1091	148–923
Mesozoo GRAZ	15–233	35–721	7–29	64–593	78–938

[1] This study, Landry et al. (2020a).
[2] Landry et al. (1998), Caron and Dennett (1999), Garrison et al. (2000), Roman et al. (2000), Barber et al. (2001), Landry (2009).
[3] Landry et al. (2021), Landry and Swalethorp (2021), Selph et al. (2021a), Yingling et al. (2021).
[4] Balch et al. (2011), Décima et al. (2011), Landry et al. (2011), Selph et al. (2011), Taylor et al. (2011).
[5] Décima et al. (2016), Freibott et al. (2016), Landry et al. (2016b), Selph et al. (2016), Taylor et al. (2016).
* Microzooplankton biomass values for the present study are underestimated relative to others because they are missing contributions of non-plastidic flagellates from epifluorescence microscopy.

on conversion of wet weight data from Tranter and Kerr (1969) to carbon equivalents and correcting for mesh size (333 μm–200 μm) according to Moriarty and O'Brien (2013). Table 2 therefore misses the upper range of values along 110°E that can be compared to systems with highly seasonal dynamics. For example, the maximum values of biomass, production and grazing for the Arabian Sea in Table 2 are from the SW monsoon upwelling season in August, and the eastern tropical Pacific study sampled the Costa Rica Dome, an analogous thermocline-ridge feature to the Java Dome (Wyrtki, 1964), during the summer upwelling peak (Landry et al., 2016a). We might expect, therefore, that the far northern edge of the 110°E transect has a seasonally shallow and rich EZ that supports biomass and production levels similar to or approaching those of the Arabian Sea and Costa Rica Dome. Such a region would reasonably have a phytoplankton community with much higher contributions of large phytoplankton cells (diatoms and dinoflagellates) than we found in the present study at the beginning of the high production season.

On the other extreme, the open waters of the Gulf of Mexico sampled during the springtime are less productive than the mean state of the eastern IO during our sampling in late austral fall, but have stronger similarities in phytoplankton community composition, including PRO dominance of biomass and production (40–65%), with relatively minor roles for diatoms and dinoflagellates (Landry et al., 2021; Selph et al., 2021). Prymnesiophytes appear to play a dominant role among eukaryotic phytoplankton in the Gulf of Mexico, which might also be the case along 110°E based on similarities the percent contributions of 19′-hexanoyloxyfucoxanthin, the prymnesiophyte-associated pigment, to total concentration of taxon-diagnostic eukaryotic carotenoids (57.9 ± 0.6%, Gulf of Mexico; Selph et al., 2021 versus 54.7 ± 0.5%; D. Antoine, unpubl.). Thus, most of the cells enumerated as EUK in our FCM analyses are likely small prymnesiophytes. Careful analysis of the oceanic subregion of the Gulf of Mexico has further shown insufficient nutrient fluxes and *in situ* productivity to support the measured zooplankton biomass and loss rate of EZ organics due to export. Both appear to be sustained by subsidies of fixed production and zooplankton transported by mesoscale eddies to open waters from the outer edges of the continental margins (Kelly et al., 2021; Landry and Swalethorp, 2021). Tranter et al. (1977) suggested something similar to explain the observed zooplankton biomass maximum in subtropical waters along 110°E during the SE monsoon, arguing that it was spatially decoupled from tropical upwelling in the Java Dome and more likely came from a closer coastal upwelling source along northwestern Australia (Rossi et al., 2003).

5. Summary and conclusions

We investigated plankton community structure and food-web dynamics from bacteria to mesozooplankton along the historic IIOE 110°E transect with the goals of 1) identifying key characteristics of its system-level trophic relationships for ecosystem modeling, 2) evaluating possible climate-driven changes in productivity since its last major study in the 1960s, 3) comparing 110°E to other similarly studied open-ocean regions. For general system characteristics, picophytoplankton, especially *Prochlorococcus*, dominated production, and microzooplankton dominated grazing, with total phytoplankton production and grazing processes tightly coupled over the transect. Strong south-to-north gradients in incident light and temperature during our sampling period had relatively little systematic effect on distributions of phytoplankton and bacterial biomass over the transect, but turnover rates (production and grazing) as well as mesozooplankton biomass displayed significant latitudinal trends. Our May–June cruise sampled the system as it was previously described, during the seasonal minimum of mesozooplankton biomass and transition to high primary productivity at the northern end. Although early methods may have underestimated productivity during IIOE, thereby masking a climate-driven decline, our contemporary estimates are similar in magnitude to the values reported for monthly estimates then and thus provide little evidence of change. While we are missing data during the periods and locations of maximum biomass accumulation to compare to other highly seasonal low-latitude systems (Arabian Sea, Costa Rica Dome) during their seasonal peaks, stocks and rate relationships along 110 °C are comparable to results from other ecosystems. Rate similarities are notable between the tropical ITF waters and central equatorial Pacific upwelling area, but phytoplankton community structure is more similar to the oceanic Gulf of Mexico. These mixed system characteristics may reflect sampling during the seasonal production transition and would be useful to corroborate during the period of peak SE monsoon forcing (August–September).

Author statement

M.R.L. and L.E.B. conceived the study. M.R.L., R.R.H., C.H.D. and D. A. conducted the field sampling and experiments. K.E.S. did the flow cytometric analyses; D.A. contributed the HPLC pigment analyses; and M.K. analyzed the microscopy samples. M.R.L. analyzed results and drafted the manuscript. All authors contributed to comments and edits of the manuscript.

Declaration of competing interest

The authors declare that they have no known competing financial interests or personal relationships that could appear to influence the work reported in this paper.

Acknowledgements

We thank the CSIRO Marine National Facility (MNF) for its support in the form of sea time on R/V *Investigator*, support personnel, scientific equipment and data management. We especially acknowledge the CSIRO hydrography/hydrochemistry team for their exceptional efforts in providing CTD and nutrient data. Greg Mitchell and Elliot Weiss provided optical expertise for the construction and calibration of the incubator boxes. Phytoplankton pigment analyses were performed by Céline Dimier and Joséphine Ras from the "Service d'Analyses de Pigments par HPLC" (SAPIGH) analytical platform of the Institut de la Mer de Villefranche (CNRS-France). Kelsey Fleming and Rasmus Swalethorp assisted with imaging and data analyses of microscopy samples. Research support was provided by National Science Foundation Grant OCE-1851558, a Murdoch University Distinguished Collaborator Award, the Hong Kong Branch of Southern Marine Science and Engineering Guangdong Laboratory (Guangzhou; SMSEGL20SC02), and the European Space Agency (PO N 5001026051). Water and plankton samples at 29-23°S, 110°E were taken under Australian Fisheries Management Authority scientific permit 1004152, Australian Government permit AU-COM2019-446 and those in the Abrolhos Marine Park under permit PA2018-00065-1 issued by the Director of National Parks, Australia. All data from the voyage are publicly available in accordance with MNF Policy. The views expressed in this publication do not necessarily represent those of the Director of National Parks, CSIRO or the Australian Government.

References

Agustí, S., González-Gordillo, J.I., Vaqué, D., Estrada, M., Cerezo, M.I., Salazar, G., Gasol, J.M., Duarte, C.M., 2015. Ubiquitous healthy diatoms in the deep sea confirm deep carbon injection by the biological pump. Nat. Commun. 6 https://doi.org/10.1038/ncomms8608.

Agustí, S., Sánchez, M.C., 2002. Cell viability in natural phytoplankton communities quantified by a membrane permeability probe. Limnol. Oceanogr. 47, 818–828.

Alldredge, A.L., 1981. The impact of appendicularian grazing on natural food concentrations in situ. Limnol. Oceanogr. 26, 247–257.

Amacher, J., Neuer, S., Lomas, M., 2013. DNA-based molecular fingerprinting of eukaryotic protists and cyanobacteria contributing to sinking particle flux at the Bermuda Atlantic time-series study. Deep Sea Res II 93, 71–83.

Ayers, J.M., Strutton, P.G., Coles, V.J., Hood, R.R., Matear, R.J., 2014. Indonesian throughflow nutrient fluxes and their potential impact on Indian Ocean productivity. Geophys. Res. Lett. 41, 5060–5506.

Azam, F., Fenchel, T., Field, G.J., Gray, J.S., Meyer-Rei1, L.A., Thingstad, F., 1983. The ecological role of water-column microbes in the sea. Mar. Ecol. Prog. Ser. 10, 257–263.

Balch, W.M., Poulton, A.J., Drapeau, D.T., Bowler, B.C., Windecker, L.A., Booth, E.S., 2011. Zonal and meridional patterns of phytoplankton biomass and carbon fixation in the Equatorial Pacific Ocean between 110°W and 140°W. Deep-Sea Res II 58, 400–416.

Barber, R.T., Marra, J., Bidigare, R., Codispoti, L., Halpern, D., Johnson, Z., Latasa, M., Goericke, R., Smith, S., 2001. Primary productivity and its regulation in the Arabian Sea during 1995. Deep Sea Res. II 48, 1127–1172.

Baudoux, A.C., Veldhuis, M.J.W., Noordeloos, A.A.M., van Noort, G., Brussaard, C.P.D., 2008. Estimates of virus vs. grazing induced mortality of picophytoplankton in the North Sea during summer. Aquat. Microb. Ecol. 52, 69–82.

Baudoux, A.C., Veldhuis, M.J., Witte, H.J., Brussaard, C.P., 2007. Viruses as mortality agents of picophytoplankton in the deep chlorophyll maximum layer during IRONAGES III. Limnol. Oceanogr. 52, 2519–2529.

Beckley, L.E., Thompson, P.A., Hood, R.R. This volume. Revisiting 110°E: a coupled biophysical, ecosystem-scale examination of Australia's International Indian Ocean Expedition line. Deep-Sea Res. II (in prep).

Behrenfeld, M.J., 2010. Abandoning sverdrup's critical depth hypothesis on phytoplankton blooms. Ecology 91, 977–989.

Bidle, K.D., 2016. Programmed cell death in unicellular phytoplankton. Curr. Biol. 26, R594–R607. https://doi.org/10.1016/j.cub.2016.05.056.

Blanchot, J., Rodier, M., 1996. Picophytoplankton abundance and biomass in the western tropical Pacific Ocean during the 1992 El Niño year: results from flow cytometry. Deep-Sea Res. I 43, 877–895.

Calbet, A., Landry, M.R., 2004. Phytoplankton growth, microzooplankton grazing and carbon cycling in marine systems. Limnol. Oceanogr. 49, 51–57.

Caron, D.A., Dennett, M.R., 1999. Phytoplankton growth and mortality during the 1995 northeast monsoon and spring intermonsoon in the Arabian Sea. Deep Sea Res. II 46, 1665–1690.

Casey, J.R., Aucan, J.P., Goldberg, S.R., Lomas, M.W., 2013. Changes in partitioning of carbon amongst photosynthetic pico- and nano-plankton groups in the Sargasso Sea in response to changes in the North Atlantic Oscillation. Deep-Sea Res. II 93, 58–70.

Chisholm, S.W., Olson, R.J., Zettler, E.R., Waterbury, J., Goericke, R., Welschmeyer, N., 1988. A novel free-living prochlorophyte occurs at high cell concentrations in the oceanic euphotic zone. Nature 334, 340–343.

Claustre, H., Bricaud, A., Babin, M., Bruyant, F., Guillou, L., Le Gall, F., Marie, D., Partensky, F., 2002. Diel variations in *Prochlorococcus* optical properties. Limnol. Oceanogr. 47, 1637–1647.

Décima, M., Landry, M.R., Rykaczewski, R.R., 2011. Broad-scale patterns in mesozooplankton biomass and grazing in the eastern equatorial Pacific. Deep-Sea Res II 58, 387–400.

Décima, M., Landry, M.R., Stukel, M.R., Lopez-Lopez, L., Krause, J.W., 2016. Mesozooplankton biomass and grazing in the Costa Rica Dome: amplifying variability through the plankton food web. J. Plankton Res. 38, 317–330.

Davies, C.H., Beckley, L.E., Richardson, A.J., n.d.. This volume. Copepods and mixotrophic Rhizaria dominate zooplankton abundances in the oligotrophic Indian Ocean. Deep-Sea Res. II. In press.

De Martini, F., Neuer, S., Hamill, D., Robidart, J., Lomas, M.W., 2018. Clade and strain specific contributions of *Synechococcus* and *Prochlorococcus* to carbon export in the Sargasso Sea. Limnol. Oceanogr. 63, S448–S457.

Deng, W., Cruz, B.N., Neuer, S., 2016. Effects of nutrient limitation on cell growth, TEP production and aggregate formation of marine *Synechococcus*. Aquat. Microb. Ecol. 78, 39–49.

Desbruyères, D., McDonagh, E.L., King, B.A., Thierry, V., 2017. Global and full-depth ocean temperature trends during the early 21st century from Argo and repeat hydrography. J. Clim. 30, 1985–1997.

DuRand, M.D., Olson, R.J., 1996. Contributions of phytoplankton light scattering and cell concentration changes to diel variations in beam attenuation in the equatorial Pacific from flow cytometric measurements of pico-, ultra- and nanoplankton. Deep Sea Res. II 43, 891–906.

Feng, M., Majewski, L.J., Fandry, C.B., Waite, A.M., 2007. Characteristics of two counter-rotating eddies in the Leeuwin Current system off the Western Australian coast. Deep-Sea Res. II 54, 961–980.

First, M.A., Miller III, H.L., Lavrentyev, P.J., Pinckney, J.L., Burd, A.B., 2009. Effects of microzooplankton growth and trophic interactions on herbivory in coastal and offshore environments. Aquat. Microb. Ecol. 54, 255–267.

Freibott, A., Taylor, A.G., Selph, K.E., Liu, H., Zhang, W., Landry, M.R., 2016. Biomass and composition of protistan grazers and heterotrophic bacteria in the Costa Rica Dome during summer 2010. J. Plankton Res. 38, 230–243.

Fuhrman, J.A., Sleeter, T.D., Carlson, C.A., Proctor, L.M., 1989. Dominance of bacterial biomass in the Sargasso Sea and its ecological implications. Mar. Ecol. Prog. Ser. 57, 207–217.

Fukuda, R., Ogawa, H., Nagata, T., Koike, I., 1998. Direct determination of carbon and nitrogen contents of natural bacterial assemblages in marine environments. Appl. Environ. Microbiol. 64, 3352–3358.

Garrison, D.L., Gowing, M.M., Hughes, M.P., Campbell, L., Caron, D.A., Dennett, M.R., Shalapyonok, A., Olson, R.J., Landry, M.R., Brown, S.L., Liu, H.-B., Azam, F., Steward, G.F., Ducklow, H.W., Smith, D.C., 2000. Microbial food web structure in the Arabian Sea: a US JGOFS study. Deep-Sea Res. II 47, 1387–1422.

Geider, R.J., MacIntyre, H.L., Kana, T.M., 1997. A dynamic model of phytoplankton growth and acclimation: responses of the balanced growth rate and the chlorophyll a:carbon ratio to light, nutrient-limitation and temperature. Mar. Ecol. Prog. Ser. 148, 187–200.

Gifford, D.J., 1988. Impact of grazing by microzooplankton in the northwest Arm of halifax harbour, nova scotia. Mar. Ecol. Prog. Ser. 47, 249–258.

Gorsky, G., Chrétiennot-Dinet, M.J., Blanchot, J., Palazzoli, I., 1999. Picoplankton and nanoplankton aggregation by appendicularians: fecal pellet contents of *Megalocerus huxleyi* in the equatorial Pacific. J. Geophys. Res. 104, 3381–3390.

Gregg, W.W., Rousseaux, C.S., 2019. Global ocean primary production trends in the modern ocean color satellite record (1998-2015). Environ. Res. Lett. 14, 124011 https://doi.org/10.1088/1748-9326/ab4667.

Guidi, L., Chaffron, S., Bittner, L., Eveillard, D., Larhlimi, A., Roux, S., Darzi, Y., Audic, S., Berline, L., Brum, J.R., Coelho, L.P., Espinoza, J.C.I., Malviya, S., Sunagawa, S., Dimier, C., Kandels-Lewis, S., Picheral, M., Poulain, J., Searson, S., Tara Oceans Consortium Coordinators, Stemmann, L., Not, F., Hingamp, P., Speich, S., Follows, M., Karp-Boss, L., Boss, E., Ogata, H., Pesant, S., Weissenbach, J., Wincker, P., Acinas, S.G., Bork, P., de Vargas, C., Iudicone, D., Sullivan, M.B., Raes, J., Karsenti, E., Bowler, C., Gorsky, G., 2016. Plankton networks driving carbon export in the oligotrophic ocean. Nature 532, 465–470.

Heldal, M., Scanlan, D., Nordland, S., Thingstad, F., Mann, F., 2003. Elemental composition of single cells of various strains of marine *Prochlorococcus* and *Synechococcus* using X-ray microanalysis. Limnol. Oceanogr. 48, 1732–1743.

Humphrey, G.F., Kerr, J.D., 1969. Seasonal variation in the Indian Ocean along 110°E. III. Chlorophylls *a* and *c*. Aust. J. Mar. Freshw. Res. 20, 55–64.

Irigoien, X., 1998. Gut clearance rate constant, temperature and initial gut contents: a review. J. Plankton Res. 20, 997–1003.

Ishizaka, J., Kiyosawa, H., Ishida, K., Ishikawa, K., Takahashi, M., 1994. Meridional distribution and carbon biomass of autotrophic picoplankton in the Central North Pacific Ocean during late northern summer 1990. Deep-Sea Res. I 41, 1745–1766.

Jitts, H.R., 1963. The simulated in situ measurement of oceanic primary production. Aust. J. Mar. Freshw. Res. 14, 139–147.

Jitts, H.R., 1969. Seasonal variation in the Indian Ocean along 110°E. IV. Primary production. Aust. J. Mar. Freshw. Res. 20, 65–75.

Johnson, P.W., Huai-Shu, X., Sieburth, J.M., 1982. The utilization of chroococcoid cyanobacteria by marine protozooplankters but not by calanoid copepods. Ann. Inst. Oceanogr. Paris Nouv. Ser. 58, 297–308.

Kelly, T.B., Landry, M.R., Selph, K.E., Knapp, A.N., Swalethorp, R., Stukel, M.R., 2021. Lateral advection supports nitrogen export in the oligotrophic open-ocean Gulf of Mexico. Nat. Commun. 12, 332. https://doi.org/10.1038/s41467-021-23678-9.

Landry, M.R., 2009. Grazing processes and secondary production in the Arabian Sea: a simple food web synthesis with measurement constraints. In: Wiggert, J.R., Hood, R. R., Naqvi, S.W.A., Brink, K.H., Smith, S.L. (Eds.), Indian Ocean: Biogeochemical Processes and Ecological Variability, vol. 185. AGU Monograph Series, pp. 133–146.

Landry, M.R., Brown, S.L., Campbell, L., Constantinou, J., Liu, H., 1998. Spatial patterns in phytoplankton growth and microzooplankton grazing in the Arabian Sea during monsoon forcing. Deep-Sea Res. II 45, 2353–2368.

Landry, M.R., Brown, S.L., Neveux, J., Dupouy, C., Blanchot, J., Christensen, S., Bidigare, R.R., 2003. Phytoplankton growth and microzooplankton grazing in high-nutrient, low-chlorophyll waters of the equatorial Pacific: community and taxon-specific rate assessments from pigment and flow cytometric analyses. J. Geophys. Res. 108 https://doi.org/10.1029/2000JC000744. C12, 8142.

Landry, M.R., Brown, S.L., Rii, Y.M., Selph, K.E., Bidigare, R.R., Yang, E.J., Simmons, M. P., 2008. Depth-stratified phytoplankton dynamics in Cyclone *Opal,* a subtropical mesoscale eddy. Deep-Sea Res. II 55, 1348–1359.

Landry, M.R., Constantinou, J., Latasa, M., Brown, S.L., Bidigare, R.R., Ondrusek, M.E., 2000. Biological response to iron fertilization in the eastern equatorial Pacific (IronEx II). III. Dynamics of phytoplankton growth and microzooplankton grazing. Mar. Ecol. Prog. Ser. 201, 57–72.

Landry, M.R., De Verneil, A., Goes, J.I., Moffett, J.W., 2016a. Plankton dynamics and biogeochemical fluxes in the Costa Rica dome: introduction to the CRD flux and zinc experiments. J. Plankton Res. 38, 167–182.

Landry, M.R., Hood, R.R., Davies, C.H., 2020a. Mesozooplankton biomass and temperature-enhanced grazing along a 110°E transect in the eastern Indian Ocean. Mar. Ecol. Prog. Ser. 649, 1–19.

Landry, M.R., Selph, K.E., Décima, M., Gutiérrez-Rodríguez, A., Stukel, M.R., Taylor, A. G., Pasulka, A.L., 2016b. Phytoplankton production and grazing balances in the Costa Rica Dome. J. Plankton Res. 38, 366–379.

Landry, M.R., Selph, K.E., Hood, R.R., Davies, C.H., Beckley, L.E., 2022. Low temperature sensitivity of picophytoplankton P:B ratios and growth rates across a natural 10°C temperature gradient in the oligotrophic Indian Ocean. Limnol. Oceanogr. Lett. 7, 112–121.

Landry, M.R., Selph, K.E., Stukel, M.R., Swalethorp, R., Kelly, T.B., Beatty, J., Quackenbush, C.R., 2021. Microbial food web dynamics in the oceanic Gulf of Mexico. J. Plankton Res. 1–18. https://doi.org/10.1093/plankt/fbab021.

Landry, M.R., Selph, K.E., Taylor, A.G., Décima, M., Balch, W.M., Bidigare, R.R., 2011. Phytoplankton growth, grazing and production balances in the HNLC equatorial Pacific. Deep-Sea Res. II 58, 524–535.

Landry, M.R., Stukel, M.R., Décima, M., 2020b. Food-web fluxes support high rates of mesozooplankton respiration and production in the equatorial Pacific. Mar. Ecol. Prog. Ser. 652, 15–32.

Landry, M.R., Swalethorp, R., 2021. Mesozooplankton biomass, grazing and trophic structure in the bluefin tuna spawning area of the oceanic Gulf of Mexico. J. Plankton Res. https://doi.org/10.1093/plankt/fbab008.

Lee, S.-K., Park, W., Baringer, M.O., Gordon, A., Huber, B., Liu, Y., 2015. Pacific origin of the abrupt increase in Indian Ocean heat content during the warming hiatus. Nat. Geosci. 8, 445–450.

Legand, M., 1969. Seasonal variations in the Indian Ocean along 110°E. VI. Macroplankton and micronekton biomass. Aust. J. Mar. Freshw. Res. 20, 85–103.

Lessard, E.J., Murrell, M.C., 1998. Microzooplankton herbivory and phytoplankton growth in the northwestern Sargasso Sea. Aquat. Microb. Ecol. 16, 173–188.

Lourey, M.J., Thompson, P.A., McLaughlin, M.J., Bonham, P., Feng, M., 2013. Primary production and phytoplankton community structure during a winter shelf-scale phytoplankton bloom off Western Australia. Mar. Biol. 160, 355–369.

Liu, H., Campbell, L., Landry, M.R., Nolla, H.A., Brown, S.L., Constantinou, J., 1998. *Prochlorococcus* and *Synechococcus* growth rates and contributions to production in the Arabian Sea during the 1995 southwest and northeast monsoons. Deep-Sea Res. II 45, 2327–2352.

Lund, J.W.G., Kipling, C., Le Cren, E.D., 1958. The inverted microscope method of estimating algal numbers and the statistical basis of estimations by counting. Hydrobiol. (Sofia) 11, 143–170.

Mackas, D., Bohrer, R., 1976. Fluorescence analysis of zooplankton gut contents and an investigation of diel feeding patterns. J. Exp. Mar. Biol. Ecol. 25, 77–85.

Marra, J., Heinemann, K.R., 1987. Primary production in the North Pacific Central Gyre: some new measurements based on ^{14}C. Deep-Sea Res. 34, 1821–1829.

Menden-Deuer, S., Lessard, E.J., 2000. Carbon to volume relationships for dinoflagellates, diatoms, and other protist plankton. Limnol. Oceanogr. 45, 569–679.

McWilliam, P.S., 1977. Further studies of plankton ecosystems in the eastern Indian Ocean. VI. Ecology of the Euphausiacea. Aust. J. Mar. Freshw. Res. 28, 627–644.

Moore, L.R., 1997. Physiological Ecology of *Prochlorococcus*: A Comparison of Isolates from Diverse Oceanic Regimes. Ph.D. Thesis. Dept. Civil and Environ. Engineering. Mass. Inst. Technol.

Monger, B.C., Landry, M.R., 1993. Flow cytometric analysis of marine bacteria with Hoechst 33342. Appl. Environ. Microbiol. 59, 905–911.

Moriarty, R., O'Brien, T., 2013. Distribution of mesozooplankton biomass in the global ocean. Earth Syst. Sci. Data 5, 45–55.

Newell, B.S., 1969. Seasonal variations in the Indian Ocean along 110°E. II. Particulate carbon. Aust. J. Mar. Freshw. Res. 20, 51–54.

Paterson, H.L., Knott, B., Waite, A.M., 2007. Microzooplankton community structure and grazing on phytoplankton, in an eddy pair in the Indian Ocean off Western Australia. Deep-Sea Res. II 54, 1076–1093.

Paterson, H.L., Knott, B., Koslow, A.J., Waite, A.M., 2008. The grazing impact of microzooplankton off south west Western Australia: as measured by the dilution technique. J. Plankton Res. 30, 379–392.

Pfannkuche, O., Lochte, K., 1993. Open ocean pelago-benthic coupling: cyanobacteria as tracers of sedimenting salp faeces. Deep-Sea Res. I 40, 727–737.

Pomroy, A., Joint, I., 1999. Bacterioplankton activity in the surface waters of the Arabian Sea during and after the 1994 SW monsoon. Deep-Sea Res. II 46, 767–794.

Putt, M., Stoecker, D.K., 1989. An experimentally determined carbon: volume ratio for marine "oligotrichous" ciliates from estuarine and coastal waters. Limnol. Oceanogr. 34, 1097–1103.

Ras, J., Claustre, H., Uitz, J., 2008. Spatial variability of phytoplankton pigment distributions in the subtropical south Pacific Ocean: comparison between in situ and predicted data. Biogeosciences 5, 353–369.

Rees, C., Pender, L., Sherrin, K., Schwanger, C., Hughes, P., Tibben, S., Marouchos, A., Rayner, M., 2018. Methods for reproducible shipboard SFA nutrient measurement using RMNS and automated data processing. Limnol Oceanogr. Methods 17, 5–41.

Rochford, D.J., 1963. Some features of organic phosphorus distribution in the south-east Indian and south-west Pacific Oceans. Aust. J. Mar. Freshw. Res. 14, 119–138.

Rochford, D.J., 1969. Seasonal variation in the Indian Ocean along 110°E. I. Hydrological structure of the upper 500 m. Aust. J. Mar. Freshw. Res. 20, 1–50.

Rochford, D.J., 1977. Further studies of plankton ecosystems in the eastern Indian Ocean. II. Seasonal variations in water mass distribution (upper 150 m) along 110°E. (August 1962-August 1963). Aust. J. Mar. Freshw. Res. 28, 541–555.

Roman, M., Smith, S., S, ., Wishner, K., Zhang, X.S., Gowing, M., 2000. Mesozooplankton production and grazing in the Arabian Sea. Deep Sea Res. II 47, 1423–1450.

Rossi, V., Feng, M., Pattiaratchi, C., Roughan, M., Waite, A.M., 2003. On the factors influencing the development of sporadic upwelling in the Leeuwin Current system. J. Geophys. Res. Oceans 118, 3608–3621.

Sakthivel, M., 1977. Further studies of plankton ecosystems in the eastern Indian Ocean. VIII. seasonal, diurnal, and latitudinal variations in abundance of Euthecosomata along the 110°E. meridian. Aust. J. Mar. Freshw. Res. 28, 663–671.

Säwström, C., Beckley, L.E., Saunders, M.I., Thompson, P.A., Waite, A.M., 2014. The zooplankton prey field for rock lobster phyllosoma larvae in relation to oceanographic features of the south-eastern Indian Ocean. J. Plankton Res. 36, 1–14.

Selph, K.E., 2021. Enumeration of marine microbial organisms by flow cytometry using near-UV excitation of Hoechst 34580-stained DNA. Limnol. Oceanogr. Methods 19, 692–701.

Selph, K.E., Landry, M.R., Taylor, A.G., Gutiérrez-Rodríguez, A., Stukel, M.R., Wokuluk, J., Pasulka, A.L., 2016. Phytoplankton production and taxon-specific growth rates in the Costa Rica Dome. J. Plankton Res. 38, 199–215.

Selph, K.E., Landry, M.R., Taylor, A.G., Yang, E.J., Measures, C.I., Yang, J.J., Stukel, M. R., Christensen, S., Bidigare, R.R., 2011. Spatially-resolved taxon-specific phytoplankton production and grazing dynamics in relation to iron distributions in the Equatorial Pacific between 110 and 140°W. Deep-Sea Res. II 58, 358–377.

Selph, K.E., Swalethorp, R., Stukel, M.R., Kelly, T.B., Knapp, A.N., Fleming, K., Hernandez, T., Landry, M.R., 2021. Phytoplankton community composition and biomass in the oligotrophic Gulf of Mexico. J. Plankton Res. https://doi.org/10.1093/plankt/fbab006.

Scheinberg, R.D., Landry, M.R., Calbet, A., 2005. Grazing of two common appendicularians on the natural prey assemblage of a tropical coastal ecosystem. Mar. Ecol. Prog. Ser. 294, 201–212.

Shalapyonok, A., Olson, R.J., Shalapyonok, L.S., 2000. Arabian sea phytoplankton during the Southwest and Northeast Monsoons 1995: composition, size structure, and biomass from individual cell properties measured by flow cytometry. Deep-Sea Res. II 48, 1231–1261.

Strickland, J.D.H., Parsons, T.R., 1972. A Practical Handbook of Seawater Analysis. Fisheries Research Board, Canada Ottawa.

Strzelecki, J., Koslow, J.A., Waite, A.M., 2007. Comparison of mesozooplankton communities from a pair of warm- and cold-core eddies off the coast of Western Australia. Deep-Sea Res. II 54, 1103–1112.

Stukel, M.R., Décima, M., Selph, K.E., Taniguchi, D.A., Landry, M.R., 2013. The role of *Synechococcus* in vertical flux in the Costa Rica upwelling dome. Prog. Oceanogr. 112, 49–59.

Sutton, A.L., Beckley, L.E., 2016. Influence of the Leeuwin Current on the epipelagic euphausiid assemblages of the south-east Indian Ocean. Hydrobiol. (Sofia) 779, 193–207.

Sverdrup, H.U., 1953. On conditions for the vernal blooming of phytoplankton. J. Cons. Internat. Explor. Mer 18, 287–295.

Talley, L.D., 1995. Preliminary results from a WHP section in the central Indian ocean. Internat. WOCE Newslett. 21, 35–38.

Taylor, A.G., Landry, M.R., Freibott, A., Selph, K.E., Gutiérrez-Rodríguez, A., 2016. Patterns of microbial community biomass, composition and HPLC diagnostic pigments in the Costa Rica upwelling dome. J. Plankton Res. 38, 183–198.

Taylor, A.G., Landry, M.R., Selph, K.E., Yang, E.J., 2011. Biomass, size structure and depth distributions of the microbial community in the eastern equatorial Pacific. Deep-Sea Res. II 58, 342–357.

Taylor, A.H., Geider, R.J., Gilbert, F.J.H., 1997. Seasonal and latitudinal dependencies of phytoplankton carbon-to-chlorophyll a ratios: results of a modelling study. Mar. Ecol. Prog. Ser. 152, 51–66.

Thompson, P.A., Wild-Allen, K., Lourey, M., Rousseaux, C., Waite, A.M., Feng, M., Beckley, L.E., 2011. Nutrients in an oligotrophic boundary current: evidence of a new role for the Leeuwin Current. Prog. Oceanogr. 91, 345–359.

Tranter, D.J., 1977a. Further studies of plankton ecosystems in the eastern Indian Ocean. V. Ecology of the Copepoda. Aust. J. Mar. Freshw. Res. 28, 593–625.

Tranter, H.A., 1977b. Further studies of plankton ecosystems in the eastern Indian Ocean. VII. The Ecology of the Amphipoda. Aust. J. Mar. Freshw. Res. 28, 645–642.

Tranter, D.J., Kerr, J.D., 1969. Seasonal variation in the Indian Ocean along 110°E. V. Zooplankton biomass. Aust. J. Mar. Freshw. Res. 20, 77–84.
Tranter, D.J., Kerr, J.D., 1977. Further studies of plankton ecosystems in the eastern Indian Ocean. III. Numerical abundance and biomass. Aust. J. Mar. Freshw. Res. 28, 557–583.
Valencia, B., Stukel, M.R., Allen, A.E., McCrow, J.P., Rabines, A., Palenik, B., Landry, M. R., 2021. Relating sinking and suspended microbial communities in the California Current Ecosystem: digestion resistance and the contributions of phytoplankton taxa to export. Environ. Microbiol. https://doi.org/10.1111/1462-2920.15736.
Vaulot, D., 1992. Estimate of phytoplankton division rates by the mitotic index method: the f_{max} approach revisited. Limnol. Oceanogr. 37, 644–649.
Vaulot, D., Marie, D., Olson, R.J., Chisholm, S.W., 1995. Growth of *Prochlorococcus*, a photosynthetic prokaryote, in the equatorial Pacific Ocean. Science 268, 1480–1482.
Veldhuis, M., Kraay, G., 2004. Phytoplankton in the subtropical Atlantic Ocean: towards a better assessment of biomass and composition. Deep-Sea Res. I 51, 507–530.
Waite, A.M., Muhling, B.A., Holl, C.M., Beckley, L.E., Montoya, J.P., Strzeleckie, J., Thompson, P.A., Pesant, S., 2007b. Food web structure in two counter-rotating eddies based on $\delta^{15}N$ and $\delta^{13}C$ isotopic analyses. Deep-Sea Res. II 54, 1055–1075.
Waite, A.M., Pesant, S., Griffin, D.A., Thompson, P.A., Holl, C.M., 2007a. Oceanography, primary production and dissolved inorganic nitrogen uptake in two Leeuwin Current eddies. Deep-Sea Res. II 54, 981–1002.
Waite, A.M., Raes, E., Beckley, L.E., Thompson, P.A., Griffin, D., Saunders, M., Säwström, C., O'Rorke, R., Wang, M., Landrum, J.P., Jeffs, A., 2019. Production and ecosystem structure in cold-core vs. warm-core eddies: implications for the zooplankton isoscape and rock lobster larvae. Limnol. Oceanogr. 64, 2405–2423.
Wang, M., O'Rorke, R., Waite, A.M., Beckley, L.E., Thompson, P., Jeffs, A.G., 2014. Fatty acid profiles of phyllosoma larvae of western rock lobster (*Panulirus cygnus*) in cyclonic and anticyclonic eddies of the Leeuwin Current off Western Australia. Prog. Oceanogr. 122, 153–162.
Waterbury, J.B., Watson, S.W., Guillard, R.R.L., Brand, L.E., 1979. Wide-spread occurrence of a unicellular, marine planktonic, cyanobacterium. Nature 277, 293–294.
Wilson, S.E., Steinberg, D.K., 2010. Autotrophic picoplankton in mesozooplankton guts: evidence of aggregate feeding in the mesopelagic zone and export of small phytoplankton. Mar. Ecol. Prog. Ser. 412, 11–27.
Woo, M., Pattiaratchi, C., 2008. Hydrography and water masses off the western Australian coast. Deep-Sea Res. I 55, 1090–1104.
Worden, A., Nolan, J., Palenik, B., 2004. Assessing the dynamics and ecology of marine picophytoplankton: the importance of the eukaryotic component. Limnol. Oceanogr. 49, 168–179.
Wyrtki, K., 1962. The upwelling in the region between Java and Australia during the south-east monsoon. Aust. J. Mar. Freshw. Res. 13, 217–225.
Wyrtki, K., 1964. Upwelling in the Costa Rica dome. Fish. Bull. 63, 355–372.
Wyrtki, K., 1973. Physical oceanography of the Indian Ocean. In: Zeitzschel, B (Ed.), Ecological studies: analysis and synthesis., vol 3 Springer, Berlin, pp. 18–36.
Yingling, N., Kelly, T.B., Selph, K.E., Landry, M.R., Knapp, A.N., Kranz, S.A., Stukel, M.R., 2021. Taxon-specific phytoplankton growth, nutrient limitation, and light limitation in the oligotrophic Gulf of Mexico. J. Plankton Res. https://doi.org/10.1093/plankt/fbab028.
Zubkov, M., Sleigh, M., Burkill, P.H., Laekey, R., 2000. Picoplankton community structure on the Atlantic Meridonal Transect: a comparison between seasons. Prog. Oceanogr. 45, 369–386.